Strongly coupled interaction between a ridge of fluid and an external airflow

C. Paterson, S. K. Wilson and B. R. Duffy

Department of Mathematics and Statistics, University of Strathclyde,

Livingstone Tower, 26 Richmond Street,

Glasgow G1 1XH, United Kingdom

(Dated: 24th July 2013)

Abstract

The behaviour of a steady thin sessile or pendent ridge of fluid on an inclined planar substrate which is strongly coupled to the external pressure gradient arising from an external airflow that flows parallel to the substrate far from the ridge is described. When the substrate is nearly horizontal a relatively large ridge can be supported against gravity by capillary and/or external pressure forces, whereas when the substrate is not restricted to being nearly horizontal only a relatively small ridge can be supported; classical thin-aerofoil theory is adapted to obtain the governing singular integro-differential equations for the profile of the ridge in each case. Attention is focused mainly on the case of a large sessile ridge on a nearly horizontal substrate. The effect of strengthening the airflow is to push a pinned ridge down near to its edges but to pull it up near to its middle. Furthermore, at a critical value of the airflow strength the upslope contact angle reaches the receding contact angle at which the upslope contact line de-pins, and continuing to increase the airflow strength beyond its critical value results in the de-pinned ridge becoming increasingly narrow, thick and symmetric in the limit of a strong external airflow. The effect of tilting the substrate is to skew a pinned ridge downslope. Furthermore, depending on the values of the advancing and receding contact angles, the ridge may first de-pin at either the upslope or the downslope contact angle but, in general, eventually both contact lines de-pin. The special cases in which only the downslope contact line de-pins and in which only the upslope contact line de-pins are also considered. It is also shown that the behavour of a large pendent ridge is qualitatively similar to that of a large sessile ridge, while the important qualitative difference between the behaviour of a large ridge and a small ridge is that, in general, for the latter one or both of the contact lines may never de-pin.

I. INTRODUCTION

The behaviour of a thin layer or droplet of viscous fluid in the presence of an external airflow has been the subject of much theoretical and experimental research because of the many practically important situations in which it occurs. In civil engineering, the interaction between the rivulets of rainwater which can form on the cables of cable-stayed bridges and the wind blowing past them is believed to play a crucial role in the rain–wind-induced vibrations of the cables (see, for example, Robertson et al. [1] and Lemaitre et al. [2]). In the electronics industry, a jet of air is sometimes used to remove droplets of water left on the surface of silicon wafers during the manufacture of microchips (see, for example, Kim et al. [3]). In the nuclear industry, careful control of the dry-out point at which the layer of water that forms on the inside surface of a steam-generating boiler pipe (through which both gas and vapour flows) completely vaporises is important for safe and efficient reactor operation (see, for, example, Cuminato et al. [4]). Other areas in which a thin layer or droplet of fluid may be subject to an external airflow include air-knife and spin-coating processes in industry (see, for example, Chou and Wu [5]) and in ice-accretion on aircraft (see, for example, Myers and Charpin [6]).

In each of the situations mentioned above, the interaction between the flow of the fluid and the external airflow passing over it plays an important role. In order to gain greater insight into and understanding of this interaction, in the present work we formulate and analyse a simple model for the strongly coupled interaction between a thin sessile or pendent ridge of fluid (or, equivalently, a two-dimensional droplet) on an inclined planar substrate and an external airflow that flows parallel to the substrate far from the ridge. Specifically, we assume that the air is inviscid and that it does not exert a shear stress on the free surface of the ridge, and adapt classical thin-aerofoil theory to obtain an expression for the pressure gradient in the air (and, in particular, for the pressure gradient on the free surface of the ridge) in terms of the unknown free surface profile of the ridge. We then use the hydrostatic equations valid within the ridge to obtain a singular integro-differential equation for the profile of the ridge

which we solve analytically in appropriate asymptotic limits and numerically.

We are not the first authors to use classical thin-aerofoil theory to tackle problems of this kind. Durbin [7] used thin-aerofoil theory to study the steady flow of a thin ridge on a horizontal substrate. Unlike in the present work, he assumed that the external airflow detaches at some point on the free surface of the ridge resulting in an asymmetric ridge profile. In particular, Durbin [7] studied the critical case in which the strength of the external airflow is at the maximum value such that the ridge is deformed but for which the contact lines do not de-pin. King and Tuck [8] used thin-aerofoil theory to study the steady flow of a thin ridge on an inclined substrate. Unlike in the present work, they included a constant shear stress at the free surface of the ridge due to the external airflow, but neglected surface tension except near to the contact lines. In particular, King and Tuck [8] found that for each value of the angle of inclination of the substrate, there are zero, one or two values of the strength of the external airflow for which a steady solution exists. Subsequently, King et al. [9] used a similar approach to study steady surface waves on a layer of fluid flowing down an inclined substrate in the absence of surface tension. Cuminato et al. [4] used thin-aerofoil theory to study the steady flow of a thin layer on a heated horizontal substrate as a model for dry-out within a steam-generating boiler pipe. Unlike in the present work, they included both a constant shear stress at the free surface of the layer and evaporative mass loss from the layer, but neglected surface tension, and, in particular, calculated the location of the dry-out point.

Although we will assume that the air is perfectly inviscid, in reality there will, of course, be viscous boundary layers at the air–substrate and the air–fluid interfaces. Smith et al. [10] showed that the pressure and shear stress due to the external airflow are comparable when the thickness of the ridge is $O(Re^{-1/8}) \ll 1$ times the boundary layer thickness, where $Re \gg 1$ is an appropriately defined Reynolds number for the airflow; the present work and that of Durbin [7], in both of which the shear stress due to the external airflow is neglected, is relevant when the thickness of the ridge is greater than $O(Re^{-1/8})$ times the boundary layer thickness.

In each of the studies mentioned above, using thin-aerofoil theory leads to a singular integro-differential equation for the unknown free surface profile of the fluid. Making analytical progress with this type of equation is not easy and techniques for solving them numerically are not routine; instead they must be treated on a problem-by-problem basis depending on the specific properties of the equation in each case, as described in the review article by Cuminato, Fitt and McKee [11] on both linear and nonlinear singular integral and integro-differential equations arising in a wide variety of physical contexts.

There have, of course, also been many other studies in which the pressure gradient and/or the shear stress due to an external airflow is prescribed rather then being coupled to the unknown free surface profile (see, for example, [12]–[26]), but these are less directly relevant to the present strongly coupled problem.

The structure of the present work is as follows. In Sec. II we use a thin-film approximation to describe the behaviour of a steady thin sessile or pendent ridge of fluid on an inclined planar substrate, including the effects of gravity and surface tension, which is strongly coupled to the external pressure gradient arising from an external airflow that flows parallel to the substrate far from the ridge, and obtain the governing singular integro-differential equations for the profile of a "large" sessile ridge on a nearly horizontal substrate, a "large" pendent ridge on a nearly horizontal substrate, and a "small" (sessile or pendent) ridge. Our attention is focused mainly on the first of these problems, namely a "large" sessile ridge on a nearly horizontal substrate. In Sec. III we describe some basic properties of the solution, while in Secs IV and V we use a combination of asymptotic and numerical techniques to analyse the effect of varying the strength of the external airflow and the angle of inclination of the substrate, respectively. Situations in which the contact lines are pinned and in which one or both of the contact lines de-pin are considered. The behaviour of the ridge in the other two problems is somewhat similar to that in the first one, and so in Secs VI and VII we consider these two problems only briefly, highlighting the qualitative similarities and differences between them and the first problem. Finally, in Sec. VIII we summarise the results obtained.

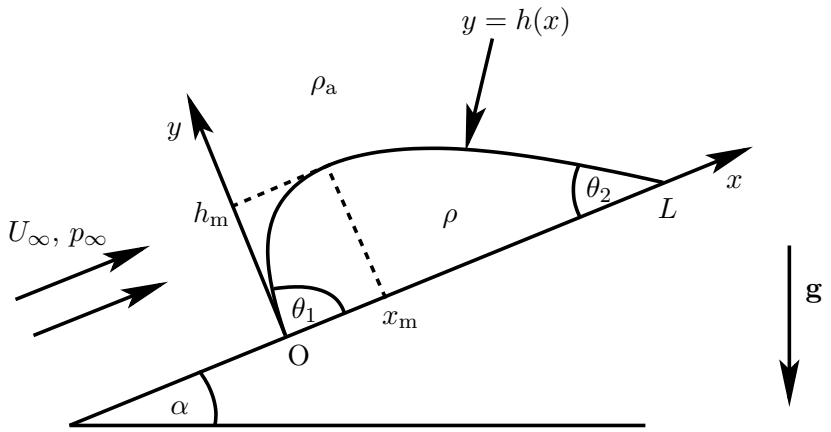

FIG. 1: Sketch of a steady thin sessile ridge of fluid on an inclined planar substrate in the presence of a steady external airflow which flows parallel to the substrate far from the ridge with constant speed U_∞ and ambient pressure p_∞.

II. PROBLEM FORMULATION

Consider a steady thin sessile or pendent ridge of fluid (or, equivalently, a two-dimensional droplet) on a planar substrate inclined at an angle α ($0 \leq \alpha \leq \pi$) to the horizontal, in the presence of a steady external airflow. Values of α satisfying $0 \leq \alpha < \pi/2$ correspond to a sessile ridge sitting on an inclined substrate as sketched in Figure 1, values of α satisfying $\pi/2 < \alpha \leq \pi$ correspond to a pendent ridge hanging from an inclined substrate, while the value $\alpha = \pi/2$ corresponds to the special case of a ridge on a vertical substrate. We assume that the fluid in the ridge has constant density ρ and coefficient of surface tension σ, and that the ridge is subject to an external flow of inviscid air of constant density ρ_a which flows parallel to the substrate far from the ridge with constant speed U_∞ and ambient pressure p_∞. The airflow is perturbed by the presence of the ridge, resulting in a non-uniform external pressure gradient that depends in a non-trivial way on the unknown free surface profile of the ridge. Referred to Cartesian coordinates Oxy with the x and y directions taken to be parallel and normal to the substrate, respectively, as indicated in Figure 1, the ridge has free surface profile $y = h(x)$ for $0 \leq x \leq L$, width L in the transverse (i.e. in the x) direction, prescribed constant volume per unit length in the longitudinal (i.e. in the z) direction V, maximum thickness $h = h_m$ at $x = x_m$, and downslope and upslope contact angles $\theta_1 = h'(0)$

(≥ 0) and $\theta_2 = -h'(L)$ (≥ 0), respectively. The pressure in both the air and the ridge is denoted by $p = p(x, y)$.

In order to analyse the problem we introduce the following non-dimensionalised and scaled variables:

$$\begin{gathered} x = L_0 x^*, \quad x_{\mathrm{m}} = L_0 x_{\mathrm{m}}^*, \quad L = L_0 L^*, \quad y = \epsilon L_0 y^*, \quad y = L_0 Y^*, \\ h = \epsilon L_0 h^*, \quad h_{\mathrm{m}} = \epsilon L_0 h_{\mathrm{m}}^*, \quad V = \epsilon L_0^2 V^*, \quad p - p_\infty = \frac{\epsilon\sigma}{L_0} p^*, \end{gathered} \tag{1}$$

where L_0 is the characteristic transverse length scale (discussed in more detail below) and $\epsilon = V/L_0^2 \ll 1$ is the (small) transverse aspect ratio of the ridge, giving $V^* = 1$ without loss of generality. Hence in what follows we set $V^* = 1$ in all of the numerical calculations, but retain V^* explicitly in all of the analytical results for clarity. Note that, since the problem has two different length scales in the y direction, two different non-dimensional y-coordinates, namely y^* and Y^*, are required. The coordinate y^* corresponding to the characteristic thickness scale for the ridge ϵL_0 ($\ll L_0$) is required to describe the behaviour of the ridge, and, in particular, the internal pressure in the ridge denoted by $p^* = p^*(x^*, y^*)$. On the other hand, the coordinate Y^* corresponding to the characteristic length scale L_0 (i.e. the same length scale as in the x-direction) is required to describe the behaviour of the external airflow, and, in particular, the external pressure in the air denoted by $p^* = P(x^*, Y^*)$. For clarity, we immediately drop the star superscripts on non-dimensional variables in what follows.

The external airflow consists of a uniform stream with constant speed U_∞ in the positive x-direction plus a non-uniform perturbation due to the presence of the ridge, which we obtain using thin-aerofoil theory (see, for example, Van Dyke [27]). The velocity potential and stream function of the external airflow $\phi(x, Y)$ and $\psi(x, Y)$ (both non-dimensionalised with $L_0 U_\infty$) are given in terms of the unknown free surface profile of the ridge by

$$\phi(x, Y) = x + \frac{\epsilon}{2\pi} \int_0^L h'(\xi) \log\left[(x - \xi)^2 + Y^2\right] \, \mathrm{d}\xi, \tag{2}$$

$$\psi(x, Y) = Y + \frac{\epsilon}{\pi} \int_0^L h'(\xi) \tan^{-1}\left(\frac{Y}{x - \xi}\right) \, \mathrm{d}\xi, \tag{3}$$

satisfying $\psi(x, 0) = 0$, where a prime denotes differentiation with respect to argument. Using

either (2) or (3) together with Bernoulli's theorem yields an expression for the leading order external pressure $P(x, Y)$, namely

$$P(x, Y) = -\Lambda \int_0^L \frac{(x-\xi)h'(\xi)}{(x-\xi)^2 + Y^2}\,\mathrm{d}\xi, \tag{4}$$

where the non-dimensional parameter Λ (≥ 0), defined by

$$\Lambda = \frac{\rho_\mathrm{a} L_0 U_\infty^2}{\pi\sigma}, \tag{5}$$

is the appropriate measure of the strength of the external airflow. Note that, since U_∞ occurs in the problem only via the term U_∞^2 in (5), the sign of U_∞ is unimportant and hence the profile of the ridge will be the same whether the external airflow is directed up or down the substrate; for definiteness we take the external airflow to be directed up the substrate, as indicated in Figure 1. Note also that, since the inviscid external airflow imposes a pressure gradient but no shear stress on the free surface of the ridge, there is no flow within the ridge. Hence, the internal pressure p satisfies the hydrostatic equations

$$\epsilon p_x = -\left(\frac{L_0}{\ell}\right)^2 \sin\alpha, \quad p_y = -\left(\frac{L_0}{\ell}\right)^2 \cos\alpha \tag{6}$$

subject to the leading order normal-stress balance at the free surface $y = h$, namely $p = P - h''$ at $Y = 0$, where $\ell = (\sigma/\rho g)^{1/2}$ denotes the usual capillary length, in which g denotes the constant magnitude of gravitational acceleration. Integrating (6b) subject to the boundary condition gives

$$p = \left(\frac{L_0}{\ell}\right)^2 (h-y)\cos\alpha + P - h''. \tag{7}$$

Substituting this solution for the internal pressure p into (6a) and evaluating the expression for the external pressure P given by (4) at $Y = 0$ yields the governing linear singular integro-differential equation for the ridge profile h, namely

$$h''' - \left(\frac{L_0}{\ell}\right)^2 h'\cos\alpha - \left(\frac{L_0}{\ell}\right)^2 \frac{\sin\alpha}{\epsilon} + \Lambda \frac{\mathrm{d}}{\mathrm{d}x}\!\!\int_0^L \frac{h'(\xi)}{x-\xi}\,\mathrm{d}\xi = 0, \tag{8}$$

where the integral is of Cauchy principal-value type. Equation (8) is to be solved subject to boundary conditions of zero thickness at both contact lines and of prescribed constant

volume, namely

$$h(0) = 0, \quad h(L) = 0, \quad V = \int_0^L h \, \mathrm{d}x. \tag{9}$$

Note that not all of the terms in (8) are necessarily of the same order in the thin-film limit $\epsilon \to 0$, and so the appropriate form of (8) depends on the particular physical situation under investigation, as described subsequently.

III. A LARGE SESSILE RIDGE

When the substrate is nearly horizontal (specifically, when $\alpha = O(\epsilon)$), the transverse component of gravity is relatively weak and so a relatively "large" ridge of width comparable to the capillary length ℓ can be supported against gravity by capillary and/or external pressure forces. In this case it is appropriate to choose $L_0 = \ell$ as the characteristic transverse length scale, so that the transverse aspect ratio is $\epsilon = V/\ell^2 \ll 1$, the characteristic pressure scale is $\epsilon\sigma/\ell = \epsilon\rho g\ell = \rho g V/\ell$, and at leading order in the limit $\epsilon \to 0$ equation (8) becomes

$$h''' - h' - \hat{\alpha} + \Lambda \frac{\mathrm{d}}{\mathrm{d}x} \fint_0^L \frac{h'(\xi)}{x - \xi} \, \mathrm{d}\xi = 0, \tag{10}$$

where

$$\Lambda = \frac{\rho_\mathrm{a} \ell U_\infty^2}{\pi\sigma} \tag{11}$$

and the non-dimensional parameter $\hat{\alpha}$ (≥ 0), defined by

$$\hat{\alpha} = \frac{\alpha}{\epsilon}, \tag{12}$$

is an appropriately scaled version of the angle of inclination of the substrate to the horizontal. Equation (10) is subject to the boundary conditions (9) and is analysed in detail below and in Secs IV and V. The corresponding equations in the pendent case (specifically, when $\pi - \alpha = O(\epsilon)$) and in the case of a small (sessile or pendent) ridge (specifically, when $\alpha = O(1)$) are derived and analysed in Secs VI and VII, respectively.

A. Local Behaviour near the Contact Lines

Local analysis of (10) reveals that near the downslope and upslope contact lines h behaves according to

$$h \sim \theta_1 x - \frac{\Lambda\theta_1}{2}x^2 \log x + \frac{\kappa_1}{2}x^2 \quad \text{as} \quad x \to 0^+ \tag{13}$$

and

$$h \sim \theta_2(L-x) - \frac{\Lambda\theta_2}{2}(L-x)^2 \log(L-x) + \frac{\kappa_2}{2}(L-x)^2 \quad \text{as} \quad x \to L^-, \tag{14}$$

respectively, where the contact angles θ_1 and θ_2 and the constants κ_1 and κ_2 are determined globally (rather than locally). In particular, (13) and (14) show that h'' (but not h or h') is logarithmically singular at both contact lines for non-zero θ_1 and θ_2.

B. Transverse Force Balance

Multiplying the governing equation (10) by h, integrating with respect to x from 0 to L, and using the local behaviour (13) and (14) yields a statement of the transverse force balance on the ridge, namely

$$\theta_1^2 - \theta_2^2 - \int_0^L \fint_0^L \frac{h'(x)h'(\xi)}{x-\xi}\,\mathrm{d}\xi\,\mathrm{d}x = 2V\hat{\alpha}. \tag{15}$$

A simple change of variables shows that the double integral in (15) is identically zero for regular (non-singular) $h'(x)$ in $0 \le x \le L$. Hence, since in the present problem, as in that studied by Durbin [7] but *not* in that studied by King and Tuck [8], there are finite contact angles at both contact lines, the transverse force balance (15) reduces to simply

$$\theta_1^2 - \theta_2^2 = 2V\hat{\alpha}, \tag{16}$$

which is equivalent to Durbin's equation (A6).

The transverse force balance (16) is a very useful relationship which (since $V > 0$ and $\hat{\alpha} \ge 0$) shows immediately that $0 \le \theta_2 \le \theta_1$, i.e. that a ridge on an inclined substrate is always skewed in the downslope direction, with $\theta_1 = \theta_2$ only in the special case of a horizontal substrate, $\hat{\alpha} = 0$. Moreover, there is a critical ridge profile which occurs when $\theta_2 = 0$ (i.e.

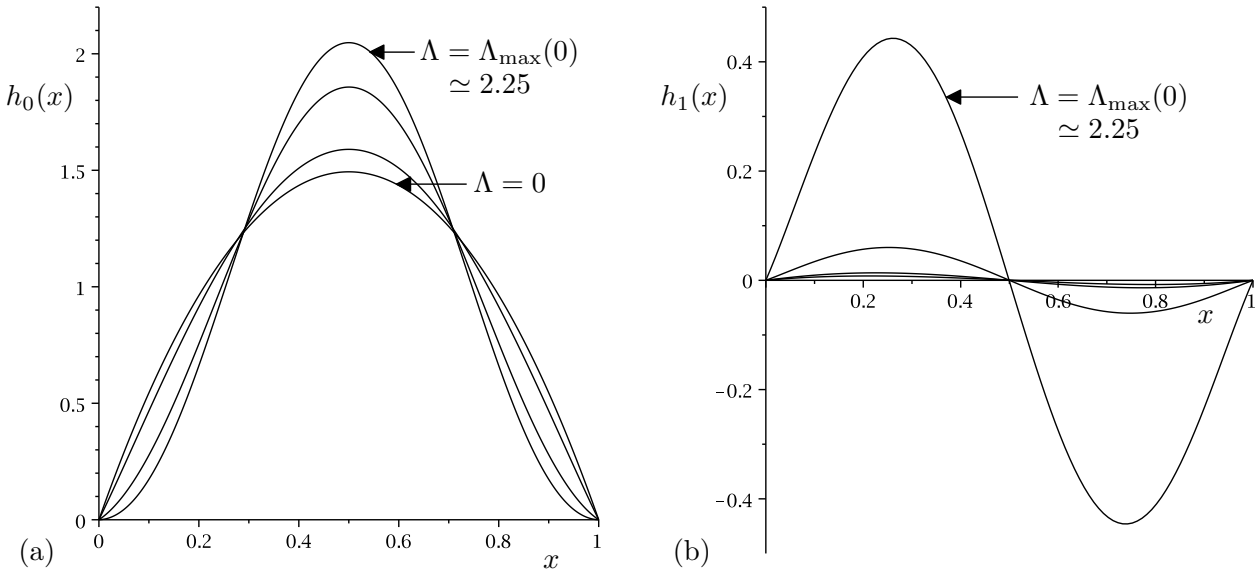

FIG. 2: Plots of the functions (a) $h_0(x)$ and (b) $h_1(x)$ appearing in the solution for the ridge profile (17) for $\Lambda = 0$, 1, 2, $\Lambda_{\max}(0) \simeq 2.25$ when $L = 1$.

when the upslope contact angle reaches its minimum physically realisable value of zero). For a prescribed value of $\hat{\alpha}$, this critical profile occurs at a critical maximum external airflow strength Λ, denoted by $\Lambda = \Lambda_{\max}(\hat{\alpha})$, above which there are no physically realisable steady solutions and, conversely, for a prescribed value of Λ, it occurs at a critical maximum angle of inclination of the substrate $\hat{\alpha}$, denoted by $\hat{\alpha} = \hat{\alpha}_{\max}(\Lambda)$, above which there are again no physically realisable steady solutions. The critical quantities $\Lambda_{\max}$ and $\hat{\alpha}_{\max}$ will be discussed further in Secs IV and V.

C. General Form of the Solution for the Ridge Profile

Inspection of (9) and (10) reveals that the general form of the solution for the ridge profile $h = h(x)$ is a linear function of V and $\hat{\alpha}$, namely

$$h = Vh_0 + \hat{\alpha}h_1, \tag{17}$$

with

$$h_0(0) = h_0(L) = h_1(0) = h_1(L) = 0, \quad \int_0^L h_0 \, \mathrm{d}x = 1, \quad \int_0^L h_1 \, \mathrm{d}x = 0, \tag{18}$$

where the function $h_0 = h_0(x)$, which represents the ridge profile in the case of a horizontal substrate $\hat{\alpha} = 0$, is positive and symmetric about $x = L/2$, and the function $h_1 = h_1(x)$ is antisymmetric about $x = L/2$. In general, we must solve (10) subject to (9) for h numerically, and we do this using the finite difference method detailed in Appendix A. Figure 2 shows numerically calculated plots of (a) h_0 and (b) h_1 when $L = 1$ for various values of Λ satisfying $\Lambda \leq \Lambda_{\max}(0) \simeq 2.25$. In particular, since h_1 is positive for $0 < x < L/2$ and negative for $L/2 < x < L$, Figure 2 shows, as might have been expected, that increasing $\hat{\alpha}$ (i.e. tilting the substrate) always skews the ridge in the downslope direction so that the maximum thickness $h_{\rm m}$ increases, the location of the maximum thickness $x_{\rm m}$ decreases (i.e. moves downslope), the downslope contact angle θ_1 increases, and the upslope contact angle θ_2 decreases.

IV. STRENGTHENING THE EXTERNAL AIRFLOW

In this section we investigate the quasi-static evolution of a large sessile ridge of prescribed constant volume V on a substrate inclined at a constant angle $\hat{\alpha}$ to the horizontal as the external airflow is gradually strengthened (i.e. as Λ is gradually increased from zero). In Sec. IV A we consider a pinned ridge with pinned contact lines, and hence constant width L but variable contact angles θ_1 and θ_2. In reality the contact lines will not remain pinned for all values of $\Lambda \leq \Lambda_{\max}$ (i.e. for all values of $\theta_2 \geq 0$). In practice (as, for example, Dussan V. [28] and Blake and Ruschak [29] describe), eventually one or both of the contact angles θ_1 and θ_2 will reach either the receding contact angle, $\theta_{\rm R}$, or the advancing contact angle, $\theta_{\rm A}$, and the corresponding contact line(s) will de-pin. For definiteness we assume that θ_1 and θ_2 satisfy $\theta_{\rm R} \leq \theta_{1,2} \leq \theta_{\rm A}$ when $\Lambda = 0$, i.e. that the ridge is always pinned in the absence of the external airflow. We will find that increasing the strength of the external airflow Λ decreases the contact angles θ_1 and θ_2, and so, while neither θ_1 nor θ_2 can ever reach $\theta_{\rm A}$, they may reach $\theta_{\rm R}$. However, as previously noted, the transverse force balance (16) shows that $\theta_2 \leq \theta_1$, and so (except in the special case $\hat{\alpha} = 0$ in which $\theta_1 = \theta_2$), θ_2 will always reach $\theta_{\rm R}$ before θ_1 does (i.e. the upslope contact line with always de-pin before the downslope one). After de-pinning we assume that θ_2 remains equal to $\theta_{\rm R}$, and hence from (16) that

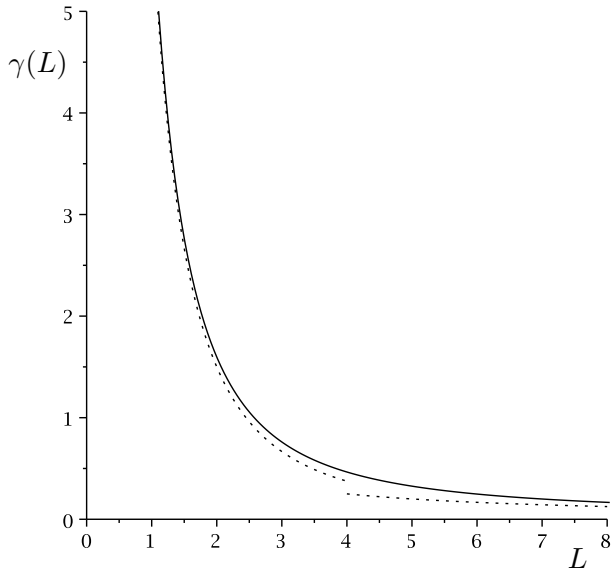

FIG. 3: Plot of the function $\gamma(L)$ given by (23). The dotted curves show the leading order asymptotic behaviour $\gamma \sim 6/L^2 \to \infty$ as $L \to 0^+$ and $\gamma \sim 1/L \to 0^+$ as $L \to \infty$.

$\theta_1 = (\theta_{\rm R}^2 + 2V\hat{\alpha})^{1/2}$ $(\geq \theta_{\rm R})$. Thus in Sec. IV B we consider a ridge that de-pins at its upslope contact line, and hence after de-pinning has variable width L but constant contact angles $\theta_1 = (\theta_{\rm R}^2 + 2V\hat{\alpha})^{1/2}$ and $\theta_2 = \theta_{\rm R}$.

A. A Pinned Ridge

In this subsection we study a pinned ridge with constant width L but variable contact angles θ_1 and θ_2 for increasing Λ.

1. *The Special Case of No External Airflow ($\Lambda = 0$)*

In the special case of no external airflow, $\Lambda = 0$, the ridge profile, denoted by $h = H_0 = H_0(x)$, is given by

$$H_0 = Vh_0 + \hat{\alpha}h_1, \tag{19}$$

where the functions $h_0 = h_0(x)$ and $h_1 = h_1(x)$ are given by

$$h_0 = \frac{\sinh\dfrac{L-x}{2}\sinh\dfrac{x}{2}}{\dfrac{L}{2}\cosh\dfrac{L}{2} - \sinh\dfrac{L}{2}} \tag{20}$$

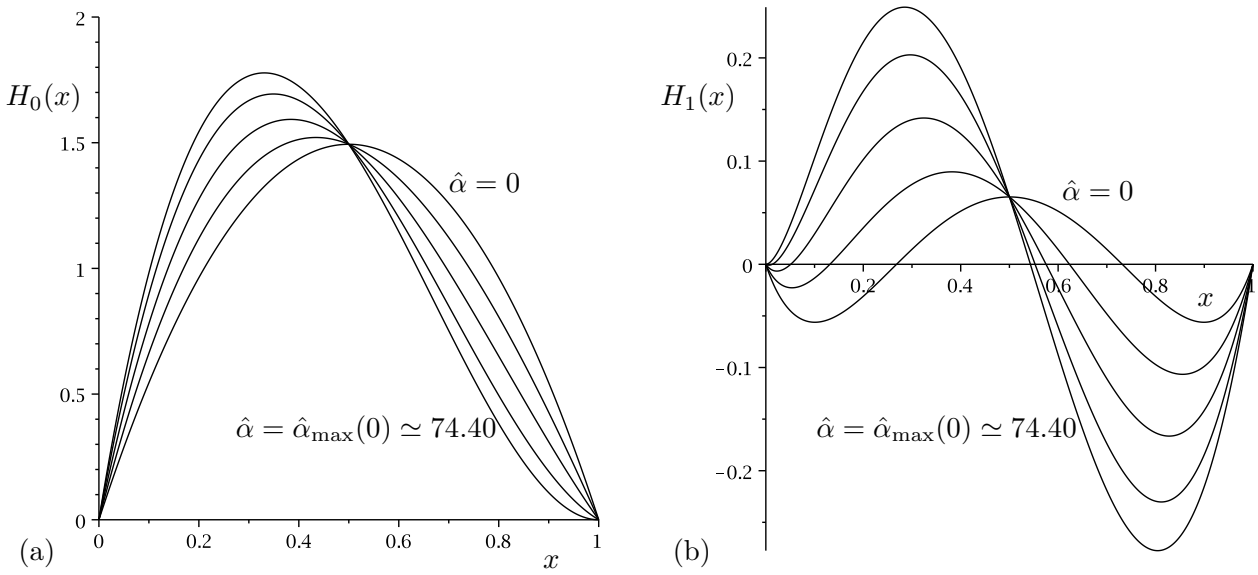

FIG. 4: Plots of (a) the leading order term, $H_0(x)$, and (b) the first order term, $H_1(x)$, in the asymptotic solution for the profile of a pinned ridge in the limit of a weak external airflow, $\Lambda \to 0^+$, given by (24) for $\hat{\alpha} = 0$, 20, 40, 60, $\hat{\alpha}_{\max}(0) \simeq 74.40$ when $L = 1$.

and

$$h_1 = \frac{L \cosh \dfrac{L-x}{2} \sinh \dfrac{x}{2}}{\sinh \dfrac{L}{2}} - x, \tag{21}$$

respectively. From (19)–(21) it may readily be deduced that the contact angles θ_1 and θ_2 are given by

$$\theta_{1,2} = V\gamma \pm \frac{\hat{\alpha}}{2\gamma}, \tag{22}$$

where the + sign is taken for θ_1, the − sign is taken for θ_2, and the function $\gamma = \gamma(L)$ (> 0) is defined by

$$\gamma = \frac{1}{2}\left(\frac{L}{2}\coth\frac{L}{2} - 1\right)^{-1}. \tag{23}$$

Inspection of (23) reveals that γ is a strictly positive, monotonically decreasing function of L and satisfies $\gamma \sim 6/L^2 \to \infty$ as $L \to 0^+$ and $\gamma \sim 1/L \to 0^+$ as $L \to \infty$, as shown in Figure 3. Hence from (22) it can be deduced that as L is increased both contact angles decrease, with θ_2 reaching zero and θ_1 reaching the non-zero value $\theta_1 = 2V\gamma = \hat{\alpha}/\gamma$ when $\hat{\alpha} = 2V\gamma^2$, and hence the critical maximum value of $\hat{\alpha}$ when $\Lambda = 0$ is given by $\hat{\alpha}_{\max}(0) = 2V\gamma^2$.

Figure 4(a) shows plots of the profile of a pinned ridge in the case of no external airflow, $H_0(x)$, for various values of $\hat{\alpha}$ when $L = 1$, in which case $\hat{\alpha}_{\max}(0) \simeq 74.40$. In particular, Figure 4(a) shows that, as previously noted, tilting the substrate skews the ridge in the downslope direction.

2. The Limit of a Weak External Airflow ($\Lambda \to 0^+$)

In the limit of a weak external airflow, $\Lambda \to 0^+$, the ridge profile takes the form

$$h = H_0 + \Lambda H_1 + O(\Lambda^2), \tag{24}$$

where the leading order term, $H_0 = H_0(x)$, is simply the solution in the special case of no external airflow, $\Lambda = 0$, given by (19)–(21) and the first order term, $H_1 = H_1(x)$, satisfies

$$H_1''' - H_1' + \frac{\mathrm{d}}{\mathrm{d}x}\fint_0^L \frac{H_0'(\xi)}{x-\xi}\,\mathrm{d}\xi = 0 \tag{25}$$

subject to

$$H_1(0) = 0, \quad H_1(L) = 0, \quad \int_0^L H_1\,\mathrm{d}x = 0. \tag{26}$$

Figure 4(b) shows numerically calculated plots of the first order term in the asymptotic solution for the profile of a pinned ridge, H_1, for various values of $\hat{\alpha}$ when $L = 1$. In the special case of a horizontal substrate, $\hat{\alpha} = 0$, H_1 is symmetric about $x = L/2$ with $H_1 > 0$ and $H_1' = 0$ at $x = x_{\mathrm{m}} = L/2$, and $-H_1'(L) = H_1'(0) < 0$. Therefore, in this case the effect of a weak external airflow is to slightly decrease both contact angles θ_1 and θ_2 equally, and to slightly increase the maximum thickness h_{m} (which always occurs at $x = x_{\mathrm{m}} = L/2$), i.e. to push the ridge down near to its edges and pull it up near to its middle. In the general case of a tilted substrate, $0 < \hat{\alpha} \leq \hat{\alpha}_{\max}$, H_1 is no longer symmetric about $x = L/2$, with $x = x_{\mathrm{m}}$ satisfying $0 < x_{\mathrm{m}} < L/2$, and $-H_1'(L) < H_1'(0) \leq 0$ with $H_1'(0) = 0$ at $\hat{\alpha} = \hat{\alpha}_{\max}(0)$. Therefore, in this case the effect of a weak external airflow is to slightly decrease both contact angles (but to decrease θ_2 more than θ_1), and to slightly increase the maximum thickness h_{m} and to move the position at which it occurs x_{m} slightly downslope, i.e. to skew the ridge downslope while simultaneously pushing it down near to its edges and pulling it up near to

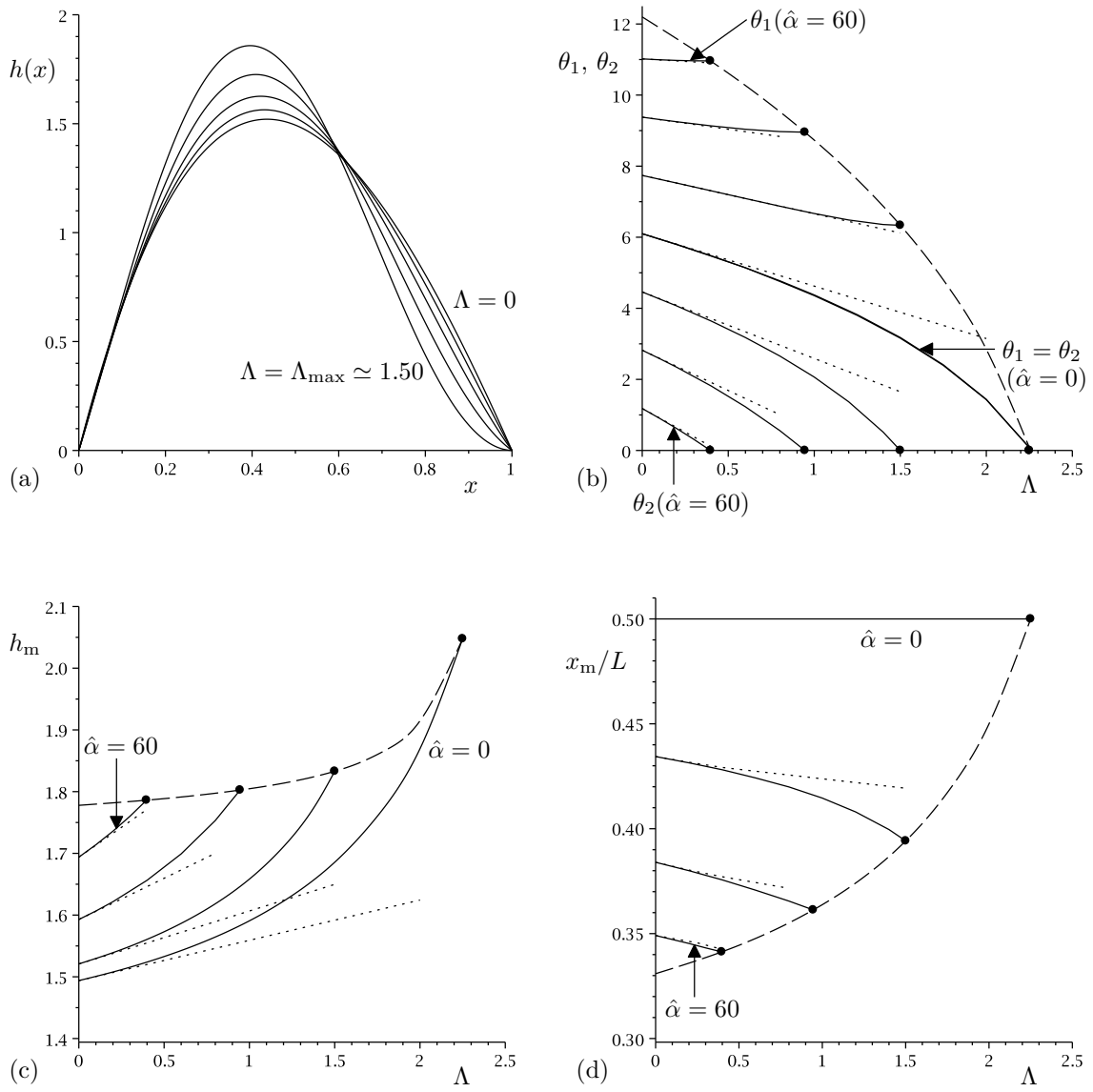

FIG. 5: Plots of (a) the profile of a large sessile pinned ridge for $\Lambda = 0$, 0.4, 0.8, 1.2, $\Lambda_{\max} \simeq 1.50$ when $\hat{\alpha} = 20$ and $L = 1$, together with plots of (b) the contact angles θ_1 and θ_2, (c) the maximum thickness $h_{\rm m}$ and (d) the relative location of the maximum thickness $x_{\rm m}/L$, as functions of Λ for a large sessile pinned ridge for $\hat{\alpha} = 0$, 20, 40, 60 when $L = 1$ (in which case $\Lambda_{\max}(0) \simeq 2.25$ and $\hat{\alpha}_{\max}(0) \simeq 74.40$). In (b)–(d) the dots indicate the points at which $\theta_2 = 0$ (i.e. when $\Lambda = \Lambda_{\max}$), the dashed lines show the curves on which $\Lambda = \Lambda_{\max}$, and the dotted lines show the first-order-accurate asymptotic solutions in the limit of a weak external airflow, $\Lambda \to 0^+$.

its middle, as in the case of a horizontal substrate. We will consider the effect of the external airflow in more detail in Sec. IV A 3 below.

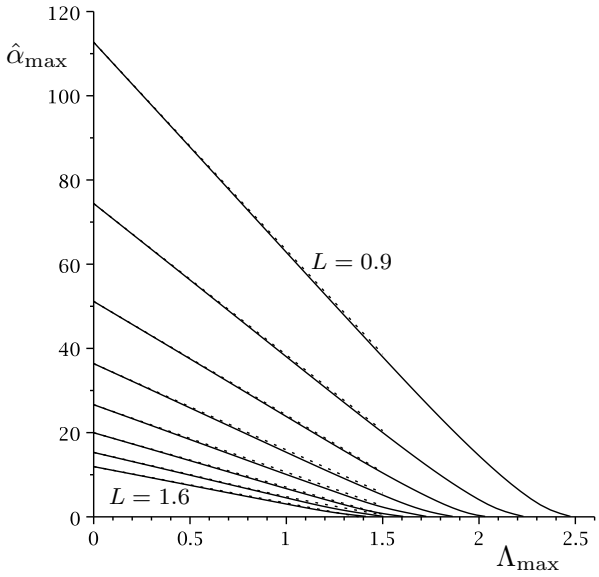

FIG. 6: Plot of the relationship between the critical inclination angle $\hat{\alpha}_{\max}$ and the critical external airflow strength $\Lambda_{\max}$ for $L = 0.9$, 1, 1.1, 1.2, 1.3, 1.4, 1.5, 1.6. The dotted lines show the first-order-accurate asymptotic solutions in the limit of a weak external airflow, $\Lambda \to 0^+$.

3. The General Case of Non-Zero External Airflow ($\Lambda > 0$)

Figure 5(a) shows plots of the profile of a pinned ridge as Λ is increased from $\Lambda = 0$ to $\Lambda = \Lambda_{\max} \simeq 1.50$ when $\hat{\alpha} = 20$ and $L = 1$. Figures 5(b)–(d) show how the contact angles θ_1 and θ_2, the maximum thickness $h_{\rm m}$ and the relative location of the maximum thickness $x_{\rm m}/L$ vary with Λ for a range of values of $\hat{\alpha}$. In particular, Figure 5(b) shows that both θ_1 and θ_2 decrease monotonically with Λ, and that $\mathrm{d}\theta_1/\mathrm{d}\Lambda = 0$ when $\theta_2 = 0$ (i.e. at $\Lambda = \Lambda_{\max}$). Furthermore, Figures 5(c) and (d) show that $h_{\rm m}$ increases monotonically and $x_{\rm m}/L$ decreases monotonically (i.e. the ridge is skewed downslope) except in the special case of a horizontal substrate, $\hat{\alpha} = 0$, in which the ridge is symmetric about $x = x_{\rm m} = L/2$ for all Λ.

Figure 6 shows the relationship between $\hat{\alpha}_{\max}$ and $\Lambda_{\max}$ (i.e. between the critical values of $\hat{\alpha}$ and Λ and for which $\theta_2 = 0$) for various values of L; this plot may be interpreted as giving either $\Lambda_{\max}$ as a function of $\hat{\alpha}$ or $\hat{\alpha}_{\max}$ as a function of Λ. In particular, Figure 6 shows that, for a given value of L, the largest possible value of $\hat{\alpha}_{\max}$ occurs at $\Lambda = 0$ (i.e. is equal to $\hat{\alpha}_{\max}(0)$), and the largest possible value of $\Lambda_{\max}$ occurs at $\hat{\alpha} = 0$ (i.e. is equal to $\Lambda_{\max}(0)$). For example, in Figures 5(b)–(d) the largest possible value of Λ is $\Lambda_{\max}(0) \simeq 2.25$, and the largest possible value of $\hat{\alpha}$ is $\hat{\alpha}_{\max}(0) \simeq 74.40$.

The results shown in Figure 5 confirm the trend evident in the limit of a weak external airflow described in Sec. IV A 2, namely that the effect of strengthening the external airflow is to skew the ridge downslope while simultaneously pushing it down near to its edges and pulling it up near to its middle. In order to understand why the external airflow has this effect on the ridge it is instructive to investigate the external pressure due to the external airflow given by (4) in more detail.

Figure 7(a) shows the external pressure at the free surface of the ridge and the substrate, $P(x,0)$, plotted as a function of x for various values of Λ when $\hat{\alpha} = 20$ and $L = 1$ (i.e. for the pinned ridge whose profile is shown in Figure 5(a)). In particular, Figure 7(a) shows that the external pressure near $x = x_{\rm m}$ is lower than the ambient pressure far from the ridge, and that the external pressure near the downslope (leading) and upslope (trailing) edges of the ridge is higher than the ambient pressure. Using the local behaviour (13) and (14) shows that near the downslope contact line P behaves according to

$$P(x,0) \sim -\Lambda\theta_1 \log x \to \infty \quad \text{as} \quad x \to 0^+ \tag{27}$$

for $\theta_1 > 0$, while near the upslope contact line P behaves according to

$$P(x,0) \sim -\Lambda\theta_2 \log(L-x) \to \infty \quad \text{as} \quad x \to L^- \tag{28}$$

for $\theta_2 > 0$ and

$$P(x,0) \sim \Lambda_{\max}\kappa_2 L = O(1) \quad \text{as} \quad x \to L^- \tag{29}$$

for $\theta_2 = 0$, i.e. a non-zero contact angle leads to a logarithmic singularity in $P(x,0)$ at the corresponding contact line. Figure 7(b) shows the external pressure, $P(x,Y)$, plotted as a function of Y for various values of x in the range $-0.3 \le x/L \le x_{\rm m}/L \simeq 0.41$ when $\Lambda = 1$, $\hat{\alpha} = 20$ and $L = 1$. In particular, Figure 7(b) shows that $P(x_{\rm m}, Y)$ is negative at $Y = 0$ and increases monotonically towards zero as Y increases. Figure 7(b) also shows that $P(0,Y)$ is large and positive near $Y = 0$ and decreases towards zero as Y increases. $P(L,Y)$ has qualitatively the same behaviour as $P(0,Y)$, but for clarity values of x/L greater than $x_{\rm m}/L \simeq 0.41$ are not shown in Figure 7(b). Figure 7(c) shows the streamlines of the external

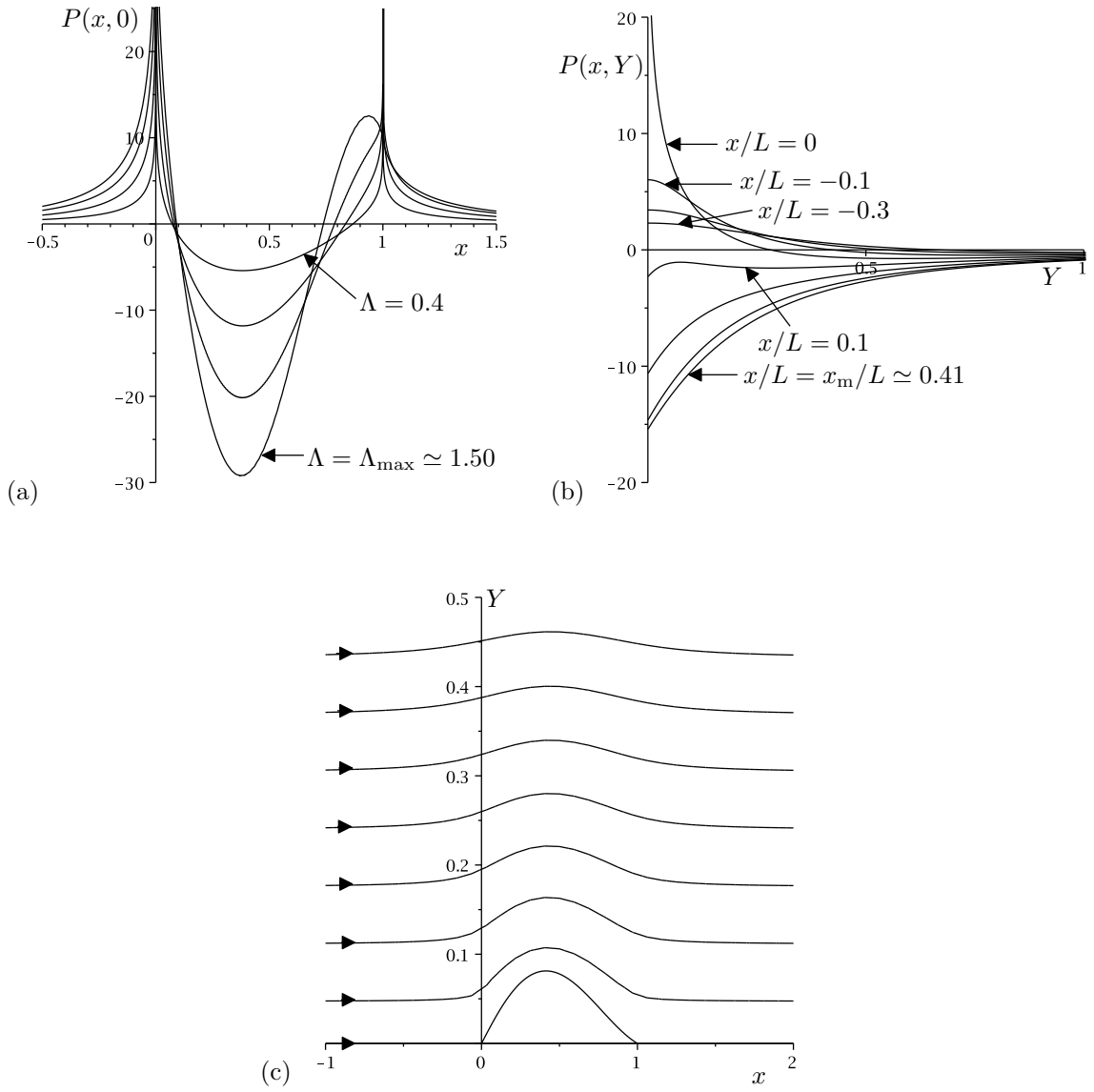

FIG. 7: Plots of (a) the external pressure at the free surface of the ridge and the substrate, $P(x,0)$, as a function of x for $\Lambda = 0$, 0.4, 0.8, 1.2, $\Lambda_{\max} \simeq 1.50$ when $\hat{\alpha} = 20$ and $L = 1$, (b) the external pressure, $P(x,Y)$, as a function of Y at $x/L = -0.3$, -0.2, -0.1, 0, 0.1, 0.2, 0.3, $x_{\rm m}/L \simeq 0.41$ when $\Lambda = 1$, $\hat{\alpha} = 20$ and $L = 1$, and (c) the streamlines of the external airflow passing over the ridge when $\Lambda = 1$, $\hat{\alpha} = 20$, $L = 1$ and $\epsilon = 0.05$.

airflow passing over the ridge plotted using (3) when $\Lambda = 1$, $\hat{\alpha} = 20$, $L = 1$ and $\epsilon = 0.05$. Far upstream and downstream of the ridge the flow is uniform and so the streamlines are parallel to the substrate, while near $x = x_{\rm m}$ the curvature of the streamlines is (slightly) negative and so, given that the pressure increases in the direction away from the centre of curvature, the pressure there is (slightly) smaller than that of the uniform stream. Hence,

the free surface tends to be pulled up near $x = x_{\rm m}$ (i.e. $h_{\rm m}$ increases). Similarly, near the contact lines the streamline curvature is (slightly) positive and so the pressure near the contact lines is (slightly) larger than that of the uniform stream. Hence, the free surface tends to be pushed down (i.e. both θ_1 and θ_2 decrease) near the contact lines.

B. A Ridge that De-Pins at its Upslope Contact Line

In this subsection we study a ridge that de-pins at its upslope contact line for increasing Λ.

As the strength of the external airflow is increased from zero the ridge initially deforms but remains pinned with constant width as described in Sec. IV A. However, since both contact angles θ_1 and θ_2 ($\leq \theta_1$) are monotonically decreasing functions of Λ, eventually at a critical external airflow strength denoted by $\Lambda = \Lambda_{\rm R}$ and satisfying $\Lambda_{\rm R} \leq \Lambda_{\rm max}$, the upslope contact angle θ_2 becomes equal to the receding contact angle $\theta_{\rm R}$ and the upslope contact line de-pins. As the strength of the external airflow is increased from $\Lambda = \Lambda_{\rm R}$ the ridge continues to deform but now with varying width L. Figure 8(a) shows plots of the profile of a de-pinned ridge as Λ is increased from $\Lambda = \Lambda_{\rm R} \simeq 1.02$ when $\hat{\alpha} = 20$ and $\theta_{\rm R} = 2$. Note that for clarity the corresponding pinned ridge profiles for $0 \leq \Lambda < \Lambda_{\rm R}$ are not shown in Figure 8(a), but examples are, of course, shown in Figure 5(a). Figures 8(b)–(e) show how the contact angles θ_1 and θ_2, the maximum thickness $h_{\rm m}$, the relative location of the maximum thickness $x_{\rm m}/L$ and the width L vary with Λ for a range of values of $\hat{\alpha}$ when $\theta_{\rm R} = 2$. Note that for $\Lambda < \Lambda_{\rm R}$ (i.e. to the left of the dots denoting the points at which the upslope contact line de-pins), the curves in Figures 8(b)–(d) are, of course, identical to the corresponding curves for a pinned ridge shown in Figures 5(b)–(d). In particular, Figure 8(b) shows that after the contact line has de-pinned (i.e. for $\Lambda > \Lambda_{\rm R}$) the contact angles $\theta_1 = (\theta_{\rm R}^2 + 2V\hat{\alpha})^{1/2}$ and $\theta_2 = \theta_{\rm R}$ are independent of the value of Λ. Moreover, Figures 8(c)–(e) show that while $h_{\rm m}$ and L are monotonically increasing and decreasing functions of Λ, respectively, $x_{\rm m}/L$ decreases to a minimum value at $\Lambda = \Lambda_{\rm R}$ before increasing towards the limiting value of

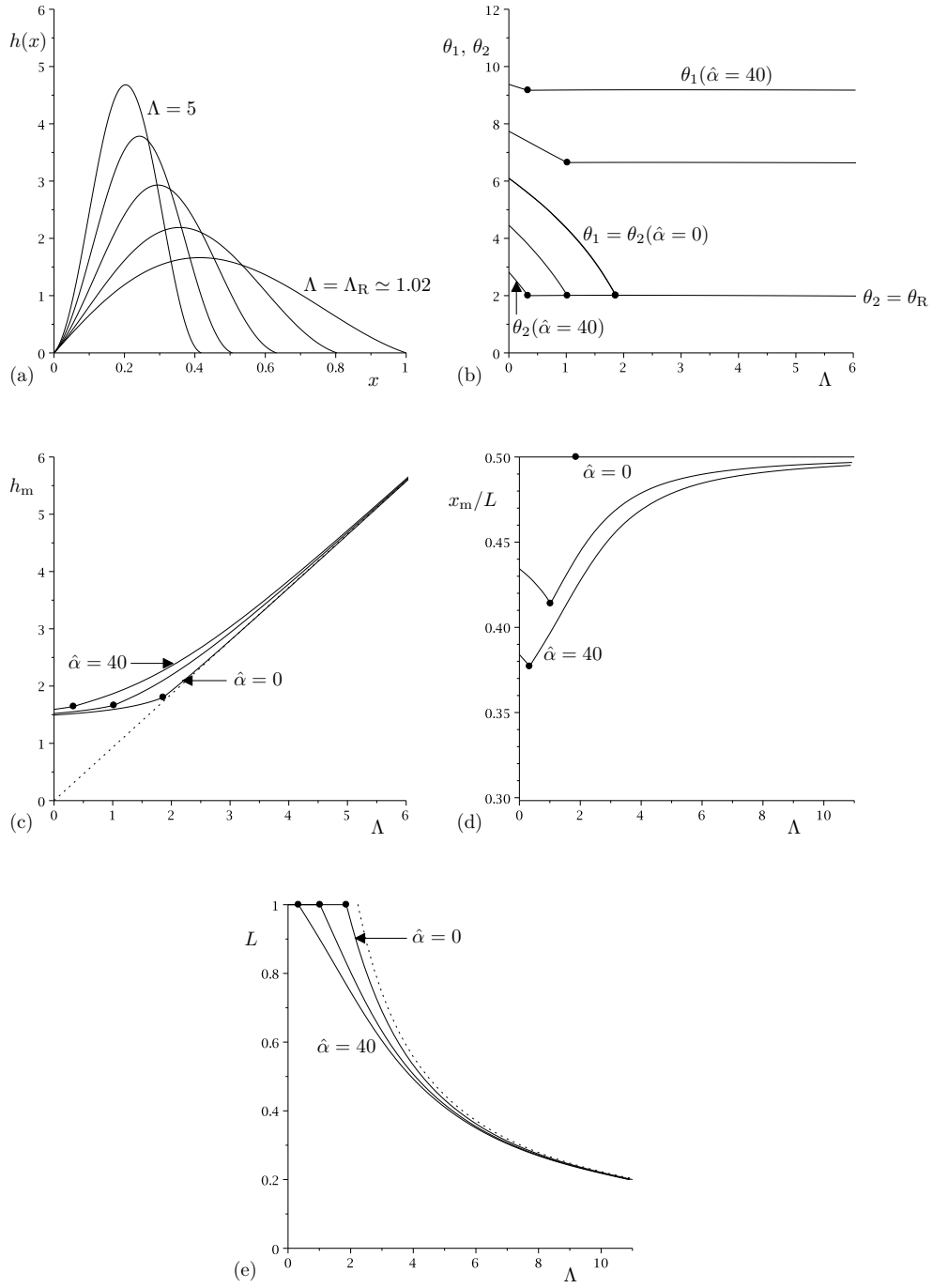

FIG. 8: Plots of (a) the profile of a large sessile de-pinned ridge for $\Lambda = \Lambda_{\rm R} \simeq 1.02$, 2, 3, 4, 5 when $\hat{\alpha} = 20$ and $\theta_{\rm R} = 2$, together with plots of (b) the contact angles θ_1 and θ_2, (c) the maximum thickness $h_{\rm m}$, (d) the relative location of the maximum thickness $x_{\rm m}/L$ and (e) the width L, as functions of Λ for a large sessile ridge whose upslope contact line de-pins for $\hat{\alpha} = 0$, 20, 40 when $\theta_{\rm R} = 2$ (in which case $\hat{\alpha}_{\rm max}(0) \simeq 50.01$). In (b)–(e) the dots indicate the points at which the upslope contact line de-pins (i.e. when $\Lambda = \Lambda_{\rm R}$ and $\theta_2 = \theta_{\rm R}$), and in (c)–(e) the dotted lines show the leading order asymptotic solutions in the limit of a strong airflow, $\Lambda \to \infty$, given by (c) $h_{\rm m} \simeq 0.94\Lambda \to \infty$, (d) $x_{\rm m}/L = 1/2$ (which coincides with the solution in the case $\hat{\alpha} = 0$) and (e) $L \simeq 2.20\Lambda^{-1} \to 0^+$ for all $\hat{\alpha}$.

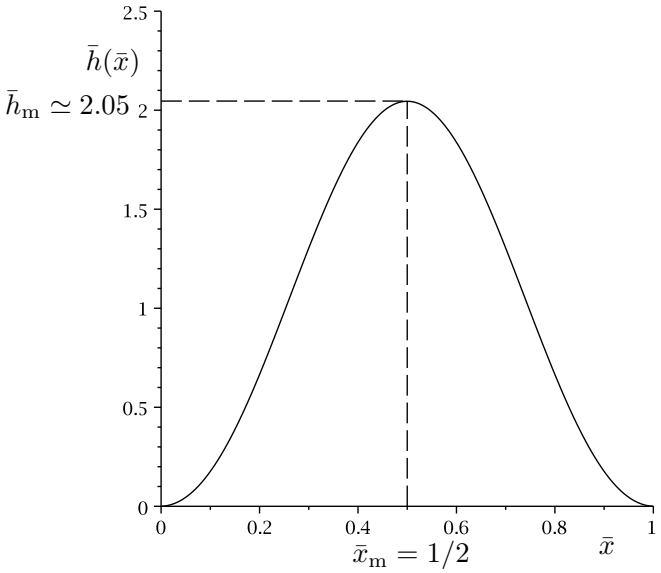

FIG. 9: Plot of the leading order scaled ridge profile $\bar{h}(\bar{x})$ in the limit of a strong external airflow, $\Lambda \to \infty$, obtained by solving (31) subject to (32) numerically.

$x_{\rm m}/L = 1/2$ as Λ becomes large.

In the limit of a strong external airflow, $\Lambda \to \infty$, the numerically calculated solutions shown in Figure 8 suggest that the ridge becomes infinitely narrow like $L = O(\Lambda^{-1}) \to 0^+$ and infinitely thick like $h_{\rm m} = O(\Lambda) \to \infty$ with $x_{\rm m}/L \to 1/2^-$. To investigate the behaviour of the ridge in this limit we therefore rescale the variables according to

$$L = \Lambda^{-1}\bar{L}, \quad x = \Lambda^{-1}\bar{L}\bar{x}, \quad x_{\rm m} = \Lambda^{-1}\bar{L}\bar{x}_{\rm m}, \quad \xi = \Lambda^{-1}\bar{L}\bar{\xi}, \quad h = \Lambda\bar{L}^{-1}\bar{h}, \quad h_{\rm m} = \Lambda\bar{L}^{-1}\bar{h}_{\rm m}, \tag{30}$$

where the scaled width $\bar{L}$ is to be determined as part of the solution. At leading order in the limit $\Lambda \to \infty$ the effect of gravity is negligible, and equations (10) and (9) become

$$\bar{h}''' + \bar{L}\frac{\mathrm{d}}{\mathrm{d}\bar{x}}\fint_0^1 \frac{\bar{h}'(\bar{\xi})}{\bar{x}-\bar{\xi}}\,\mathrm{d}\bar{\xi} = 0 \tag{31}$$

subject to

$$\bar{h}(0) = 0, \quad \bar{h}(1) = 0, \quad \bar{h}'(1) = 0, \quad \int_0^1 \bar{h}\,\mathrm{d}\bar{x} = V. \tag{32}$$

Equation (31) was solved subject to (32) numerically to obtain the solution for the leading order scaled ridge profile $\bar{h} = \bar{h}(\bar{x})$, and, in particular, the leading order values $\bar{L} \simeq 2.20$, $\bar{h}_{\rm m} \simeq 2.05$ and $\bar{x}_{\rm m} = 1/2$. Figure 9 shows $\bar{h}$ plotted as a function of $\bar{x}$, and, in particular,

shows that $\bar{h}$ is symmetric about $\bar{x} = \bar{x}_{\rm m} = 1/2$. The leading order asymptotic solutions for $h_{\rm m} \simeq 0.94\Lambda \to \infty$ and $L \simeq 2.20\Lambda^{-1} \to 0^+$ are shown with dotted lines in Figures 8(c) and (e), while in Figure 8(d) the leading order asymptotic solution for $x_{\rm m}/L = 1/2$ coincides with the solution in the case $\hat{\alpha} = 0$. In particular, this asymptotic solution shows how the ridge becomes infinitely narrow, thick and symmetric in the limit of a strong external external airflow. While this asymptotic solution is formally valid for arbitrarily large values of Λ, the underlying thin-film approximation will, of course, eventually fail when Λ becomes too large.

V. TILTING THE SUBSTRATE

In this section we investigate the quasi-static evolution of a large sessile ridge of prescribed constant volume V in the presence of an external airflow of constant strength Λ as the substrate is gradually tilted (i.e. as the angle of inclination of the substrate $\hat{\alpha}$ to the horizontal is gradually increased from zero). Like in Sec. IV A, in Sec. V A we again consider a pinned ridge with pinned contact lines, and hence constant width L but variable contact angles θ_1 and θ_2. However, unlike in Sec. IV A, in which we found that increasing Λ decreases both θ_1 and θ_2, we will find that increasing $\hat{\alpha}$ increases θ_1 and decreases θ_2; moreover, as the general form of the solution for the ridge profile (17) shows, both θ_1 and θ_2 vary linearly with $\hat{\alpha}$. Like in Sec. IV, in reality the contact lines will not remain pinned for all values of $\hat{\alpha} \leq \hat{\alpha}_{\rm max}$ (i.e. for all values of $\theta_2 \geq 0$). In practice, either θ_1 will reach $\theta_{\rm A}$ or θ_2 will reach $\theta_{\rm R}$ and the corresponding contact line(s) will de-pin. For definiteness we assume that θ_1 and θ_2 satisfy $\theta_{\rm R} \leq \theta_{1,2} \leq \theta_{\rm A}$ when $\hat{\alpha} = 0$, i.e. that the ridge is always pinned when the substrate is horizontal. However, unlike in Sec. IV, in which, in general, θ_2 always reaches $\theta_{\rm R}$ first as Λ is increased, now it is possible *either* for θ_2 to reach $\theta_{\rm R}$ first *or* for θ_1 to reach $\theta_{\rm A}$ first as $\hat{\alpha}$ is increased. After de-pinning we assume that either θ_2 remains equal to $\theta_{\rm R}$ and hence from (16) that $\theta_1 = (\theta_{\rm R}^2 + 2V\hat{\alpha})^{1/2}$ $(\geq \theta_{\rm R})$ is an increasing function of $\hat{\alpha}$, or θ_1 remains equal to $\theta_{\rm A}$ and hence from (16) that $\theta_2 = (\theta_{\rm A}^2 - 2V\hat{\alpha})^{1/2}$ $(\leq \theta_{\rm A})$ is a decreasing function of $\hat{\alpha}$, as appropriate. In Sec. V B we consider the general situation in which both contact lines

eventually de-pin, while in Secs V C and V D we consider the special cases in which only the downslope contact line de-pins and only the upslope contact line de-pins, respectively.

A. A Pinned Ridge

Figure 10(a) shows plots of the profile of a pinned ridge as $\hat{\alpha}$ is increased from $\hat{\alpha} = 0$ to $\hat{\alpha}_{\rm max} \simeq 38.02$ when $\Lambda = 1$ and $L = 1$. Figures 10(b)–(d) show how θ_1, θ_2, $h_{\rm m}$ and $x_{\rm m}/L$ vary with $\hat{\alpha}$ for a range of values of Λ. In particular, Figure 10(b) shows that θ_1 increases linearly and θ_2 decreases linearly with $\hat{\alpha}$. Furthermore, Figures 10(c) and (d) show that $h_{\rm m}$ increases monotonically and $x_{\rm m}/L$ decreases monotonically with $\hat{\alpha}$ (i.e. the ridge is skewed downslope as the substrate is tilted). Note that, as in Figures 5(b)–(d) discussed previously in Sec. IV A, in Figures 10(b)–(d) (which correspond to the same values of L and V) the largest possible value of Λ is $\Lambda_{\rm max}(0) \simeq 2.25$, and the largest possible value of $\hat{\alpha}$ is $\hat{\alpha}_{\rm max}(0) \simeq 74.40$.

B. A Ridge that Eventually De-Pins at Both of its Contact Lines

In the general case in which $\theta_{\rm A}$ is finite and $\theta_{\rm R}$ is non-zero, the ridge eventually de-pins at both of its contact lines for increasing $\hat{\alpha}$, but the order in which the contact lines de-pin depends on the value of Λ. Specifically, if θ_1 reaches $\theta_{\rm A}$ at some value $\hat{\alpha} = \hat{\alpha}_{\rm A}(\Lambda)$ ($< \hat{\alpha}_{\rm max}(\Lambda)$), before θ_2 reaches $\theta_{\rm R}$, then the downslope contact line will de-pin first, but if θ_2 reaches $\theta_{\rm R}$ at some value $\hat{\alpha} = \hat{\alpha}_{\rm R}(\Lambda)$ ($< \hat{\alpha}_{\rm max}(\Lambda)$), before θ_1 reaches $\theta_{\rm A}$, then the upslope contact line will de-pin first. Regardless of which contact line de-pins first, the second contact line de-pins when *both* $\theta_1 = \theta_{\rm A}$ *and* $\theta_2 = \theta_{\rm R}$, and hence from the transverse force balance (16) this always occurs at $\hat{\alpha} = \hat{\alpha}_{\rm AR}$, where

$$\hat{\alpha}_{\rm AR} = \frac{\theta_{\rm A}^2 - \theta_{\rm R}^2}{2V}, \tag{33}$$

which is independent of the value of Λ, and for $\hat{\alpha} > \hat{\alpha}_{\rm AR}$ there are no steady solutions of the kind considered here. There is a critical value of Λ, denoted by $\Lambda_{\rm AR}$, for which the two contact lines de-pin simultaneously (i.e. $\theta_1 = \theta_{\rm A}$ and $\theta_2 = \theta_{\rm R}$ simultaneously for the first time at $\hat{\alpha} = \hat{\alpha}_{\rm AR}$). The value of Λ relative to $\Lambda_{\rm AR}$ determines which of the two contact

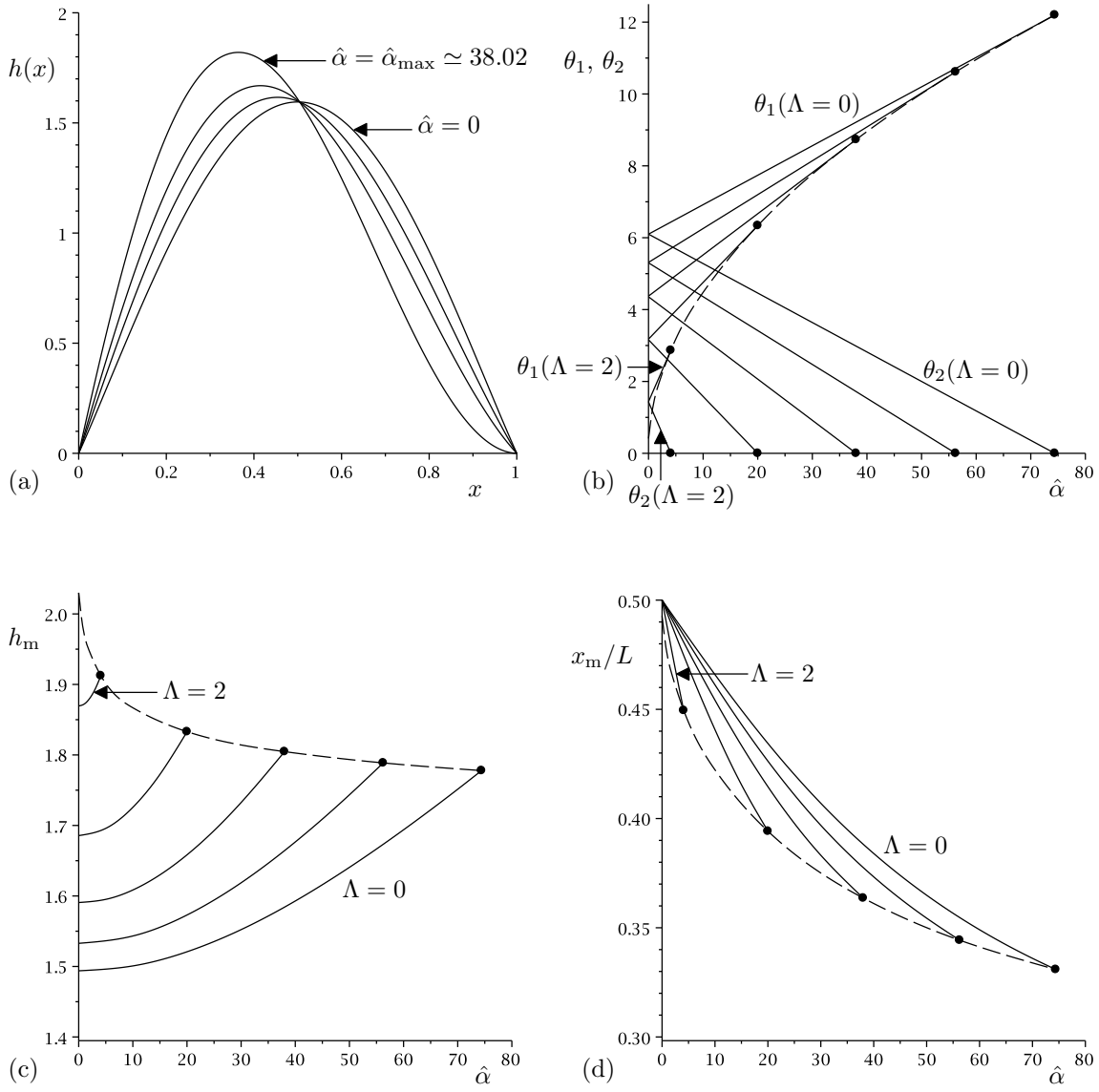

FIG. 10: Plots of (a) the profile of a large sessile pinned ridge for $\hat{\alpha} = 0$, 10, 20, $\hat{\alpha}_{\max} \simeq 38.02$ when $\Lambda = 1$ and $L = 1$, together with plots of (b) the contact angles θ_1 and θ_2, (c) the maximum thickness $h_{\rm m}$ and (d) the relative location of the maximum thickness $x_{\rm m}/L$, as functions of $\hat{\alpha}$ for a large sessile pinned ridge for $\Lambda = 0$, 0.5, 1, 1.5 and 2 when $L = 1$ (in which case $\Lambda_{\max}(0) \simeq 2.25$ and $\hat{\alpha}_{\max}(0) \simeq 74.40$). In (b)–(d) the dots indicate the points at which $\theta_2 = 0$ (i.e. when $\hat{\alpha} = \hat{\alpha}_{\max}$) and the dashed lines show the curves on which $\hat{\alpha} = \hat{\alpha}_{\max}$.

lines de-pins first for increasing $\hat{\alpha}$: specifically, if $\Lambda < \Lambda_{\rm AR}$ then the downslope contact line de-pins first, while if $\Lambda > \Lambda_{\rm AR}$ then the upslope contact line de-pins first.

Figure 11(a) and 11(b) show plots of the profile of a ridge as $\hat{\alpha}$ is increased from $\hat{\alpha} = 0$ to $\hat{\alpha} = \hat{\alpha}_{\rm AR} = 45/2 = 22.50$ in the cases $\Lambda < \Lambda_{\rm AR} \simeq 0.93$ and $\Lambda > \Lambda_{\rm AR}$, respectively, when

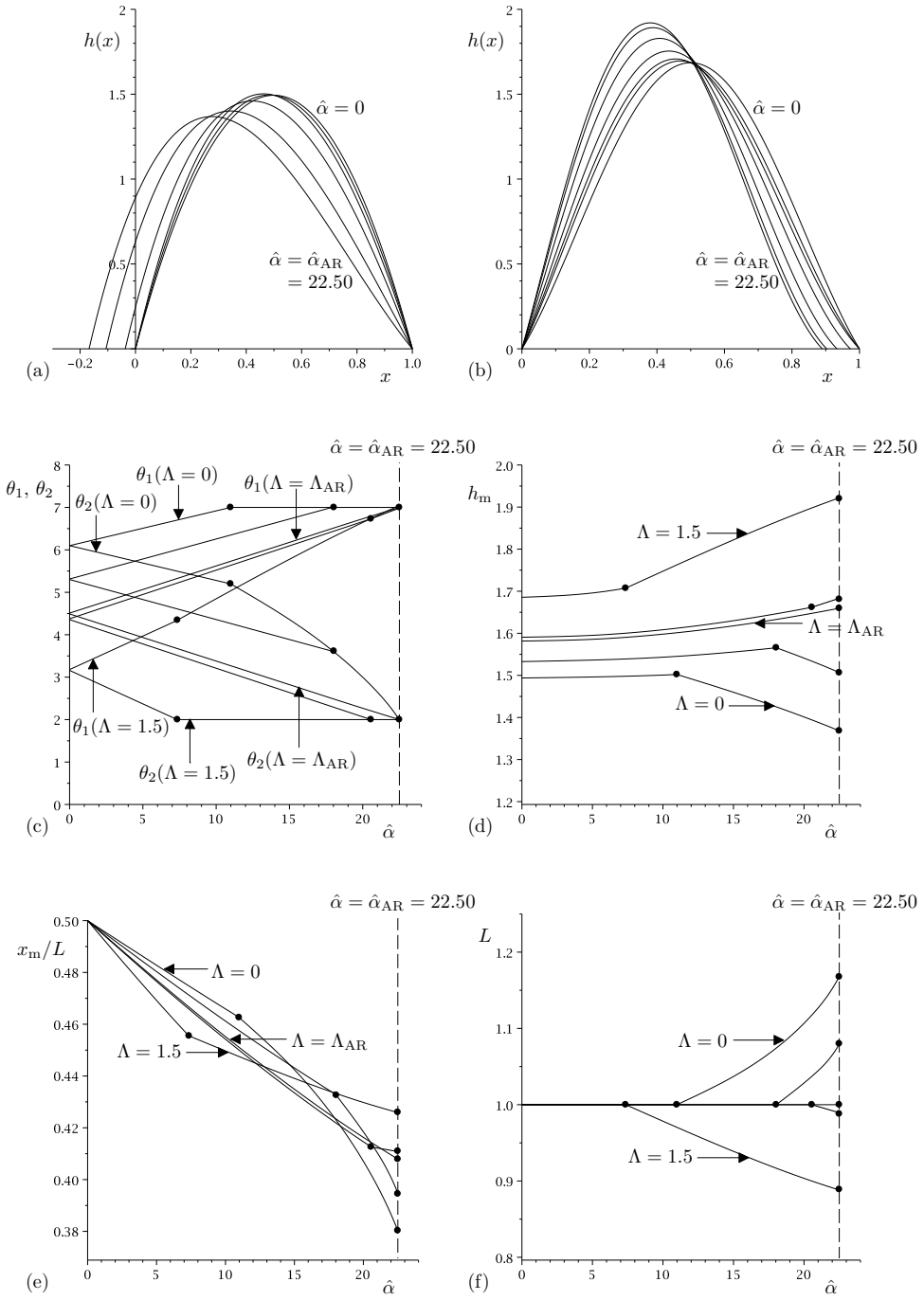

FIG. 11: Plots of (a) the profile of a large sessile ridge that first de-pins at its downslope contact line for $\hat{\alpha} = 0$, 5, $\hat{\alpha}_{\rm A} \simeq 10.99$, 15, 20, $\hat{\alpha}_{\rm AR} = 22.50$ when $\Lambda = 0$ ($< \Lambda_{\rm AR} \simeq 0.93$), $\theta_{\rm A} = 7$ and $\theta_{\rm R} = 2$, (b) the profile of a large sessile ridge that first de-pins at its upslope contact line for $\hat{\alpha} = 0$, 5, $\hat{\alpha}_{\rm R} \simeq 7.34$, 10, 15, 20, $\hat{\alpha}_{\rm AR} = 22.50$ when $\Lambda = 1.5$ ($> \Lambda_{\rm AR}$), $\theta_{\rm A} = 7$ and $\theta_{\rm R} = 2$, together with plots of (c) the contact angles θ_1 and θ_2, (d) the maximum thickness $h_{\rm m}$, (e) the relative location of the maximum thickness $x_{\rm m}/L$, and (f) the width L, as functions of $\hat{\alpha}$ for a large sessile ridge whose upslope and downslope contact lines de-pin for $\Lambda = 0$, 0.5, $\Lambda_{\rm AR} \simeq 0.93$, 1, 1.5 when $\theta_{\rm A} = 7$ and $\theta_{\rm R} = 2$. In (c)–(f) the leftmost dot on each curve indicates the point at which the first contact line (which can be either the upslope or downslope contact line) de-pins, the rightmost dot indicates the point $\hat{\alpha} = \hat{\alpha}_{\rm AR}$ at which the second contact line de-pins, and the vertical dashed line indicates the value $\hat{\alpha} = \hat{\alpha}_{\rm AR} = 22.50$ beyond which there are no steady solutions of the kind considered here.

$\theta_{\rm A} = 7$ and $\theta_{\rm R} = 2$. Figures 11(c)–(f) show how θ_1 and θ_2, $h_{\rm m}$, $x_{\rm m}/L$ and L vary with $\hat{\alpha}$ for a range of values of Λ when $\theta_{\rm A} = 7$ and $\theta_{\rm R} = 2$. Note that until the first contact line de-pins (i.e. to the left of the leftmost dots denoting the points at which the first contact line de-pins), the curves in Figures 11(c)–(e) are, of course, identical to the corresponding curves for a pinned ridge shown in Figures 10(b)–(d). In particular, Figures 11(c) and (f) show that if $\Lambda < \Lambda_{\rm AR}$ then the downslope contact line de-pins first and the width of the ridge increases after de-pinning, if $\Lambda > \Lambda_{\rm AR}$ then the upslope contact line de-pins first and the width of the ridge decreases after de-pinning, and if $\Lambda = \Lambda_{\rm AR}$ then the two contact lines de-pin simultaneously.

C. A Ridge that De-Pins Only at its Downslope Contact Line

In the special case when $\theta_{\rm R} = 0$ the upslope contact line remains pinned for all values of $\theta_2 \geq 0$, while the downslope contact line de-pins at $\hat{\alpha} = \hat{\alpha}_{\rm A}$. Figure 12(a) shows plots of the profile of a ridge which has de-pinned at its downslope contact line as $\hat{\alpha}$ is increased from $\hat{\alpha} = \hat{\alpha}_{\rm A} \simeq 23.08$ to $\hat{\alpha} = \hat{\alpha}_{\rm Amax} = 49/2 = 24.50$ when $\Lambda = 1$, $\theta_{\rm A} = 7$ and $\theta_{\rm R} = 0$. Figures 12(b)–(e) show how θ_1 and θ_2, $h_{\rm m}$, $x_{\rm m}/L$ and L vary with $\hat{\alpha}$ for a range of values of Λ when $\theta_{\rm A} = 7$ and $\theta_{\rm R} = 0$. In particular, Figure 12(e) shows that the width of the ridge always increases after de-pinning. The upslope contact angle eventually reaches the value $\theta_2 = \theta_{\rm R} = 0$ when $\theta_{\rm A}^2 = 2V\hat{\alpha}$, and so, as Figures 12(b)–(e) show, there is a maximum value of $\hat{\alpha} = \hat{\alpha}_{\rm Amax} = \theta_{\rm A}^2/2V$ ($= \hat{\alpha}_{\rm AR}$ evaluated at $\theta_{\rm R} = 0$), which is independent of the value of Λ, at which the ridge achieves its maximum width and beyond which there are no steady solutions of the kind considered here.

D. A Ridge that De-Pins Only at its Upslope Contact Line

In the special case when $\theta_{\rm A} = \infty$ the downslope contact line remains pinned for all values of θ_1, while the upslope contact line de-pins at $\hat{\alpha} = \hat{\alpha}_{\rm R}$. Figure 13(a) shows plots of the profile of a ridge which has de-pinned at its upslope contact line as $\hat{\alpha}$ is increased from

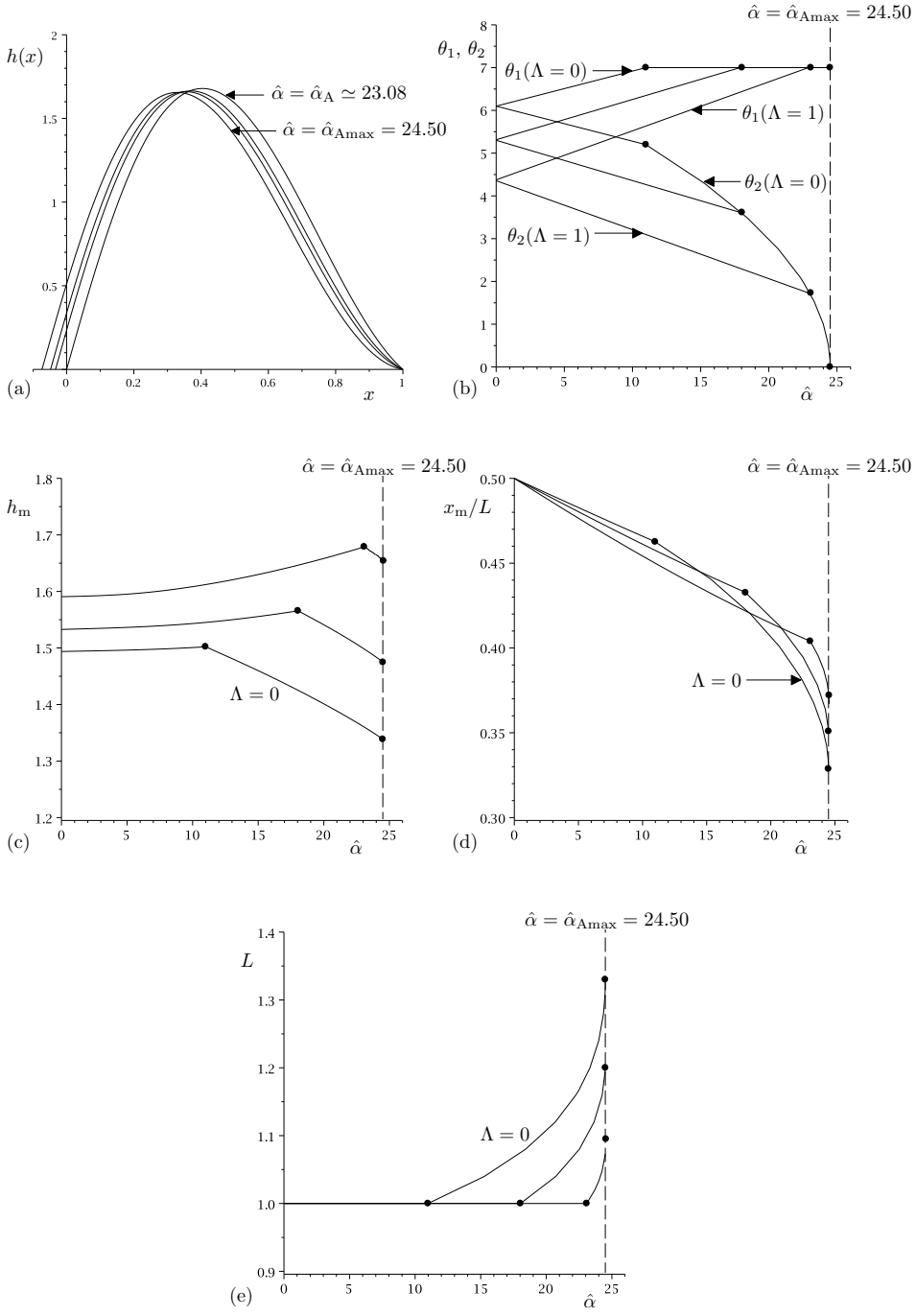

FIG. 12: Plots of (a) the profile of a large sessile ridge which has de-pinned at its downslope contact line for $\hat{\alpha} = \hat{\alpha}_{\rm A} \simeq 23.08$, 24, 24.25, $\hat{\alpha}_{\rm Amax} = 24.50$ when $\Lambda = 1$, $\theta_{\rm A} = 7$ and $\theta_{\rm R} = 0$, together with plots of (b) the contact angles θ_1 and θ_2, (c) the maximum thickness $h_{\rm m}$, (d) the relative location of the maximum thickness $x_{\rm m}/L$ and (e) the width L, as functions of $\hat{\alpha}$ for a large sessile ridge whose downslope contact line de-pins for $\Lambda = 0$, 0.5, 1 when $\theta_{\rm A} = 7$ and $\theta_{\rm R} = 0$. In (b)–(e) the leftmost dot on each curve indicates the point at which the downslope contact line de-pins, the rightmost dot indicates the point $\hat{\alpha} = \hat{\alpha}_{\rm Amax}$ at which $\theta_2 = 0$, and the vertical dashed line indicates the value $\hat{\alpha} = \hat{\alpha}_{\rm Amax} = 24.50$ beyond which there are no steady solutions on the kind considered here.

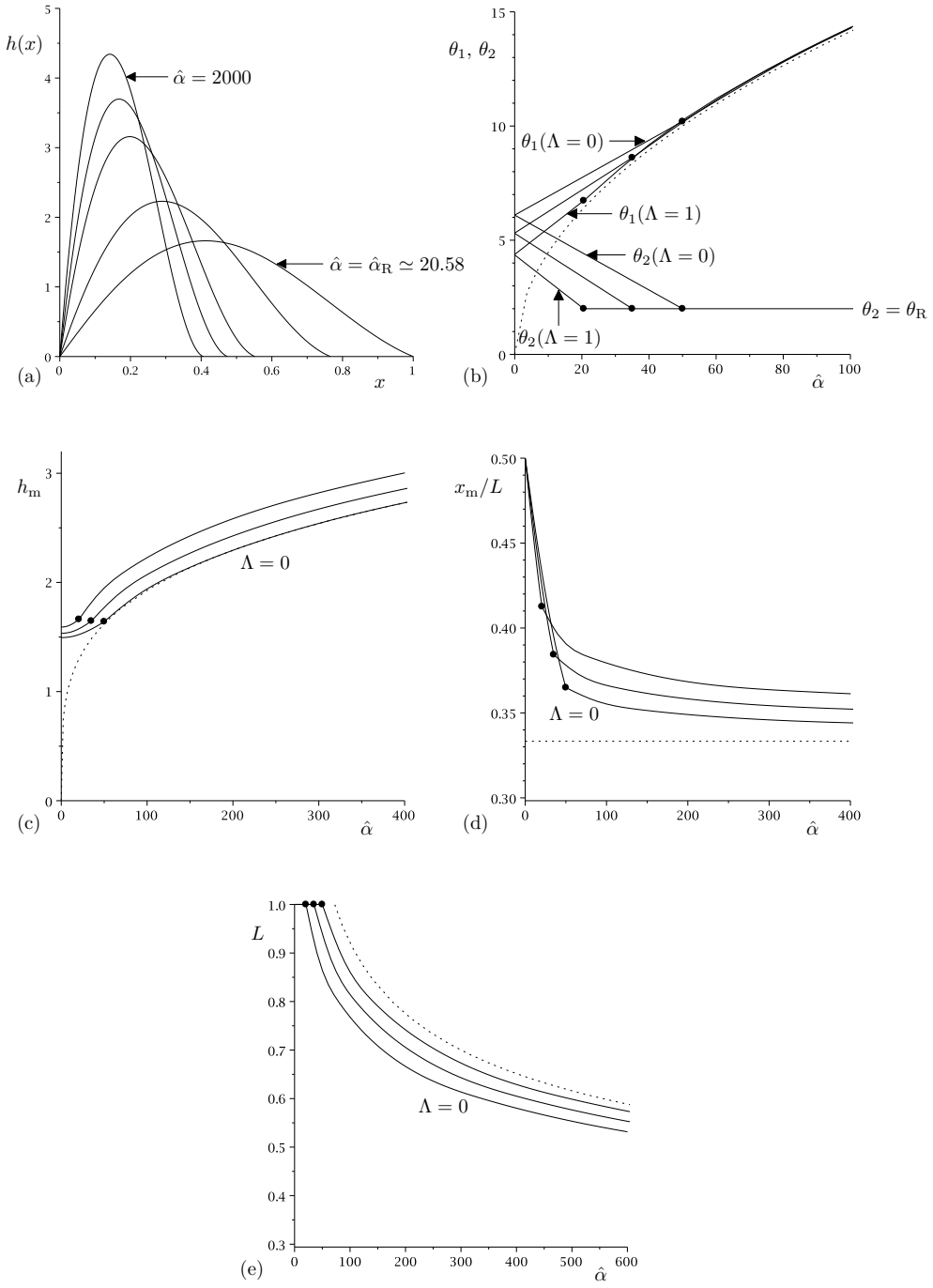

FIG. 13: Plots of (a) the profile of a large sessile ridge which has de-pinned at its upslope contact line for $\hat{\alpha} = \hat{\alpha}_{\rm R} \simeq 20.58$, 100, 500, 1000, 2000 when $\Lambda = 1$, $\theta_{\rm A} = \infty$ and $\theta_{\rm R} = 2$, together with plots of (b) the contact angles θ_1 and θ_2, (c) the maximum thickness $h_{\rm m}$, (d) the relative location of the maximum thickness $x_{\rm m}/L$ and (e) the width L, as functions of $\hat{\alpha}$ for a large sessile ridge whose upslope contact line de-pins for $\Lambda = 0$, 0.5, 1 when $\theta_{\rm A} = \infty$ and $\theta_{\rm R} = 2$. In (b)–(e) the dots on each curve indicate the point at which the upslope contact line de-pins, and the dotted curves show the leading order asymptotic solutions in the limit of a large angle of inclination of the substrate, $\hat{\alpha} \to \infty$, given by (b) $\theta_1 \simeq 1.41\hat{\alpha}^{1/2} \to \infty$, (c) $h_{\rm m} \simeq 0.61\hat{\alpha}^{1/4} \to \infty$, (d) $x_{\rm m}/L \to 1/3^+$ and (e) $L \simeq 2.91\hat{\alpha}^{-1/4} \to 0^+$ for all Λ.

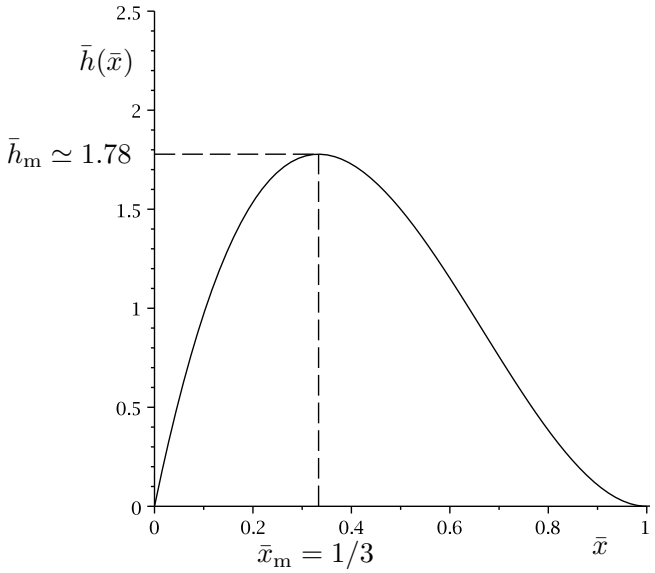

FIG. 14: Plot of the scaled ridge profile $\bar{h}(\bar{x})$ in the limit of a large angle of inclination of the substrate, $\hat{\alpha} \to \infty$, given by (37) and (38).

$\hat{\alpha} = \hat{\alpha}_{\rm R} \simeq 20.58$ when $\Lambda = 1$, $\theta_{\rm A} = \infty$ and $\theta_{\rm R} = 2$. Figures 13(b)–(e) show how θ_1 and θ_2, $h_{\rm m}$, $x_{\rm m}/L$ and L vary with $\hat{\alpha}$ for a range of values of Λ when $\theta_{\rm A} = \infty$ and $\theta_{\rm R} = 2$. In particular, Figure 13(e) shows that the width of the ridge always decreases after de-pinning.

In the limit of a large angle of inclination of the substrate, $\hat{\alpha} \to \infty$, the numerically calculated solutions shown in Figure 13 suggest that the ridge becomes infinitely narrow like $L = O(\hat{\alpha}^{-1/4}) \to 0^+$ and infinitely thick like $h_{\rm m} = O(\hat{\alpha}^{1/4}) \to \infty$ with $x_{\rm m}/L \to 1/3^+$. To investigate the behaviour of the ridge in this limit we therefore rescale the variables according to

$$\begin{gathered} L = \hat{\alpha}^{-1/4}\bar{L}, \quad x = \hat{\alpha}^{-1/4}\bar{L}\bar{x}, \quad x_{\rm m} = \hat{\alpha}^{-1/4}\bar{L}\bar{x}_{\rm m}, \quad \xi = \hat{\alpha}^{-1/4}\bar{L}\bar{\xi}, \\ h = \hat{\alpha}^{1/4}\bar{L}^{-1}\bar{h}, \quad h_{\rm m} = \hat{\alpha}^{1/4}\bar{L}^{-1}\bar{h}_{\rm m}, \quad \theta_1 = \hat{\alpha}^{1/2}\bar{L}^{-2}\bar{\theta}_1, \end{gathered} \tag{34}$$

where the scaled width $\bar{L}$ is to be determined as part of the solution. At leading order in the limit $\hat{\alpha} \to \infty$ the effects of the external airflow and of the normal component of gravity are negligible, and equations (10) and (9) become

$$\bar{h}''' - \bar{L}^4 = 0 \tag{35}$$

subject to

$$\bar{h}(0) = 0, \quad \bar{h}(1) = 0, \quad \bar{h}'(1) = 0, \quad \int_0^1 \bar{h}\,{\rm d}\bar{x} = V. \tag{36}$$

Equations (35) and (36) have the simple exact solution

$$\bar{h} = \frac{\bar{L}^4}{6}\bar{x}(1-\bar{x})^2 = 12V\bar{x}(1-\bar{x})^2, \quad \text{where} \quad \bar{L} = (72V)^{1/4} \simeq 2.91V^{1/4}, \tag{37}$$

which gives the values

$$\bar{\theta}_1 = \frac{\bar{L}^4}{6} = 12V, \quad \bar{h}_{\rm m} = \frac{2\bar{L}^4}{81} = \frac{16V}{9} \simeq 1.78V, \quad \bar{x}_{\rm m} = \frac{1}{3}. \tag{38}$$

Figure 14 shows $\bar{h}$ plotted as a function of $\bar{x}$, and, in particular, shows that $\bar{h}$ is skewed downslope with $\bar{x}_{\rm m} = 1/3$. The leading order asymptotic solutions for $\theta_1 = (2V\hat{\alpha})^{1/2} \simeq 1.41\hat{\alpha}^{1/2} \to \infty$, $\theta_2 = 0$, $h_{\rm m} = (16/9)(V^3\hat{\alpha}/72)^{1/4} \simeq 0.61\hat{\alpha}^{1/4} \to \infty$, $x_{\rm m}/L = 1/3$ and $L = (72V/\hat{\alpha})^{1/4} \simeq 2.91\hat{\alpha}^{-1/4} \to 0^+$ are shown with dotted lines in Figures 13(b)–(e). In particular, this asymptotic solution shows how the ridge becomes infinitely narrow and thick and is skewed downslope with infinitely large downslope contact angle in the limit of a large angle of inclination of the substrate. Like the solution in the limit of strong external airflow discussed in Sec. IV B, while this asymptotic solution is formally valid for arbitrarily large values of $\hat{\alpha}$, the underlying thin-film approximation will, of course, eventually fail when $\hat{\alpha}$ becomes too large.

VI. A LARGE PENDENT RIDGE

The equation for the profile of a large pendent ridge on a nearly horizontal substrate (specifically, when $\pi - \alpha = O(\epsilon)$), differs from the corresponding equation for a large sessile ridge (10) derived in Sec. III only in the sign of the h' term (i.e. the term corresponding to the normal component of gravity), where Λ is again given by (11) and $\hat{\alpha}$ (≥ 0) is now defined by

$$\hat{\alpha} = \frac{\pi - \alpha}{\epsilon}. \tag{39}$$

This equation is again subject to the boundary conditions (9), and equations (13)–(18) again hold.

In the special case of no external airflow, $\Lambda = 0$, the ridge profile is again given by (19),

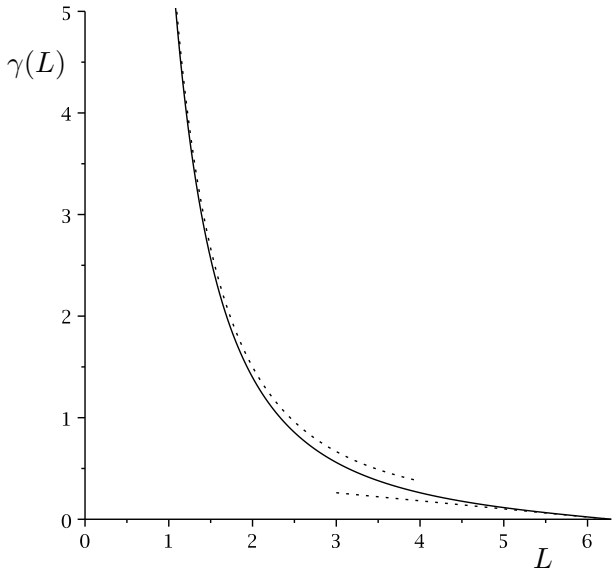

FIG. 15: Plot of the function $\gamma(L)$ given by (42). The dotted curves show the leading order asymptotic behaviour $\gamma \sim 6/L^2 \to \infty$ as $L \to 0^+$ and $\gamma \sim (2\pi - L)/4\pi \to 0^+$ as $L \to 2\pi^-$.

where the functions $h_0 = h_0(x)$ and $h_1 = h_1(x)$ are now given by

$$h_0 = \frac{\sin\dfrac{L-x}{2}\sin\dfrac{x}{2}}{\sin\dfrac{L}{2} - \dfrac{L}{2}\cos\dfrac{L}{2}} \tag{40}$$

and

$$h_1 = x - \frac{L\cos\dfrac{L-x}{2}\sin\dfrac{x}{2}}{\sin\dfrac{L}{2}}, \tag{41}$$

respectively. The contact angles θ_1 and θ_2 are again given by (22), where the function $\gamma = \gamma(L)$ is now defined by

$$\gamma = \frac{1}{2}\left(1 - \frac{L}{2}\cot\frac{L}{2}\right)^{-1}. \tag{42}$$

Inspection of (42) reveals that, unlike for a sessile ridge (23), for a pendent ridge γ has multiple branches of solutions. However, γ is a strictly positive, monotonically decreasing function of L in the only interval in which the solutions for h are physically realisable, namely $0 < L \leq 2\pi$, and satisfies $\gamma \sim 6/L^2 \to \infty$ as $L \to 0^+$ and $\gamma \sim (2\pi - L)/4\pi \to 0^+$ as $L \to 2\pi^-$, as shown in Figure 15.

The quasi-static evolution of a large pendent ridge as the external airflow is gradually strengthened and as the substrate is gradually tilted is similar to that of a large sessile ridge

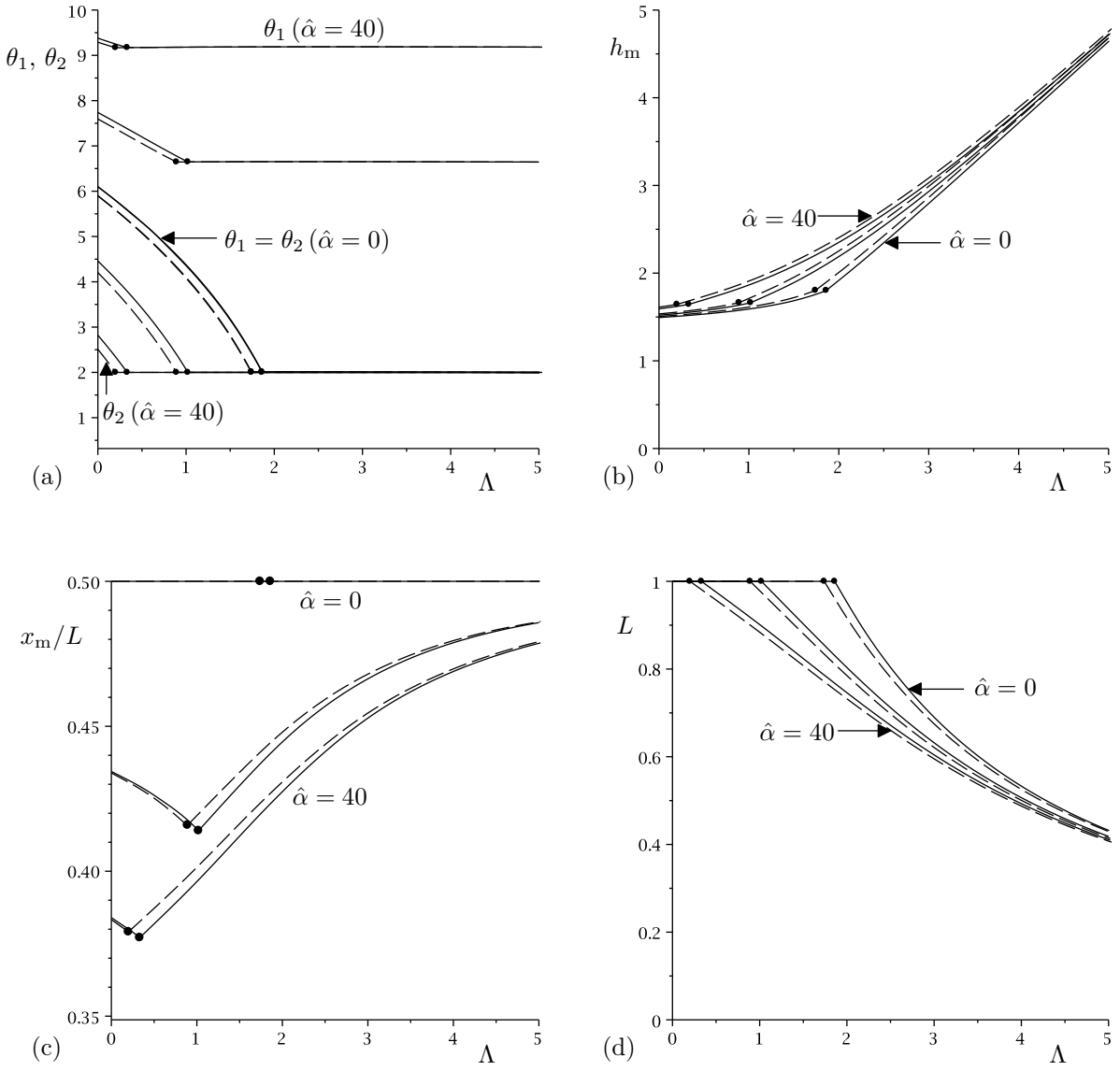

FIG. 16: Plots of (a) the contact angles θ_1 and θ_2, (b) the maximum thickness $h_{\rm m}$, (c) the relative location of the maximum thickness $x_{\rm m}/L$, and (d) the width L, as functions of Λ for a large pendent ridge whose upslope contact line de-pins for $\hat{\alpha}=0$, 20, 40 when $\theta_{\rm R}=2$. The dots indicate the points at which the upslope contact line de-pins (i.e. when $\Lambda=\Lambda_{\rm R}$ and $\theta=\theta_{\rm R}$). The solid lines show the results for a large sessile ridge for which $\hat{\alpha}=\alpha/\epsilon$ and the dashed lines show the results for a large pendent ridge for which $\hat{\alpha}=(\pi-\alpha)/\epsilon$.

described in Secs IV and V, respectively. For example, Figure 16 shows how θ_1, θ_2, $h_{\rm m}$, $x_{\rm m}/L$ and L vary with Λ for a range of values of $\hat{\alpha}$ when $\theta_{\rm R}=2$ for both a large sessile and a large pendent ridge. In particular, Figure 16 shows that the behaviour of the two ridges is qualitatively similar, with the pendent ridge (shown with the dashed lines) generally

being slightly thicker, de-pinning at a slightly smaller value of $\Lambda_{\rm R}$, and (after de-pinning occurs) being slightly narrower than the corresponding sessile ridge (shown with the solid lines). Moreover, as Figure 16 also shows, at leading order in the limit of a strong external airflow, $\Lambda \to \infty$, the effect of gravity is negligible and both sessile and pendent ridges behave according to the asymptotic solution described in Sec. IV B.

VII. A SMALL (SESSILE OR PENDENT) RIDGE

When the substrate is not restricted to being nearly horizontal (specifically, when $\alpha = O(1)$), in both sessile and pendent cases the transverse component of gravity is relatively strong and so only a relatively "small" ridge of width much less than the capillary length ℓ can be supported against gravity by capillary and/or external pressure forces. In this case it is appropriate to choose $L_0 = \sqrt{\epsilon}\ell = V^{1/4}\sqrt{\ell}$ as the characteristic transverse length scale, so that the aspect ratio is $\epsilon = \sqrt{V}/\ell \ll 1$, the characteristic pressure scale is $\sqrt{\epsilon}\sigma/\ell = \sqrt{\epsilon}\rho g\ell = \rho g V^{1/4}\sqrt{\ell}$, and at leading order in the limit $\epsilon \to 0$ equation (8) becomes

$$h''' - \sin\alpha + \Lambda \frac{\mathrm{d}}{\mathrm{d}x}\int_0^L \frac{h'(\xi)}{x-\xi}\,\mathrm{d}\xi = 0, \tag{43}$$

where

$$\Lambda = \frac{\rho_{\rm a}\sqrt{\epsilon}\ell U_\infty^2}{\pi\sigma} = \frac{\rho_{\rm a} V^{1/4}\sqrt{\ell} U_\infty^2}{\pi\sigma}. \tag{44}$$

This equation is again subject to the boundary conditions (9), the local behaviour near the contact lines is again given by (13) and (14), the transverse force balance is simply

$$\theta_1^2 - \theta_2^2 = 2V\sin\alpha, \tag{45}$$

and the general form of the solution for the ridge profile is $h = Vh_0 + \sin\alpha\, h_1$, where the functions $h_0 = h_0(x)$ and $h_1 = h_1(x)$ again satisfy (18). Comparing equation (43) with the corresponding equation for a large ridge (10) reveals, as might have been expected, that the normal component of gravity is negligible for a small ridge, and hence that the leading order solutions for a small sessile and a small pendent ridge are identical. Moreover, comparing the definitions of Λ for large and small ridges (given by equations (11) and (44), respectively)

reveals that the external airflow required to support even a small ridge on a substrate which is not nearly horizontal is stronger than that required to support a large ridge on a nearly horizontal substrate (specifically, U_∞ must be larger by a factor of $\epsilon^{-1/4} = (\ell/\sqrt{V})^{1/4} \gg 1$).

In the special case of no external airflow, $\Lambda = 0$, the ridge profile, denoted by $h = H_0 = H_0(x)$, is given by $H_0 = V h_{00} + \sin\alpha\, h_{01}$, where the functions $h_{00} = h_{00}(x)$ and $h_{01} = h_{01}(x)$ are given by

$$h_{00} = \frac{6x(L-x)}{L^3} \tag{46}$$

and

$$h_{01} = \frac{x}{12}(L-x)(L-2x), \tag{47}$$

respectively, and the contact angles θ_1 and θ_2 are given by

$$\theta_{1,2} = \frac{6V}{L^2} \pm \frac{L^2 \sin\alpha}{12}, \tag{48}$$

where again the + sign is taken for θ_1 and the − sign is taken for θ_2. In particular, from (48) it can immediately be deduced that as L is increased both contact angles decrease, just as they do in the case of a large ridge discussed in Secs III–VI. However, since, unlike the value of $\hat{\alpha}$, the value of $\sin\alpha$ cannot exceed unity, unlike in the case of a large ridge in which θ_2 always reaches zero for sufficiently large values of L, for a small ridge θ_2 reaches zero and θ_1 reaches the non-zero value $\theta_1 = 12V/L^2 = (L^2 \sin\alpha)/6$ when $\sin\alpha = 72V/L^4$ only if $72V/L^4 \leq 1$ with both θ_1 and θ_2 remaining strictly positive and taking the minimum values $\theta_{1,2} = 6V/L^2 \pm L^2/12$ when $\sin\alpha = 72V/L^4 = 1$ otherwise. Note that the present solution for a small ridge in the special case of no external airflow was first obtained (albeit with a slightly different scaling) by Hocking and Miksis [30]. In the limit of a weak external airflow, $\Lambda \to 0^+$, the ridge profile again takes the form (24), where the leading order term, $H_0 = H_0(x)$, is again simply the solution in the special case of no external airflow, $\Lambda = 0$, and the first order term, $H_1 = H_1(x)$, is given by $H_1(x) = V h_{10} + \sin\alpha\, h_{11}$, where the functions $h_{10} = h_{10}(x)$ and $h_{11} = h_{11}(x)$ are given by

$$h_{10} = \log L - \frac{5x(L-x)}{2L^2} - \frac{x^2(3L-2x)}{L^3}\log x - \frac{(L-x)^2(L+2x)}{L^3}\log(L-x) \tag{49}$$

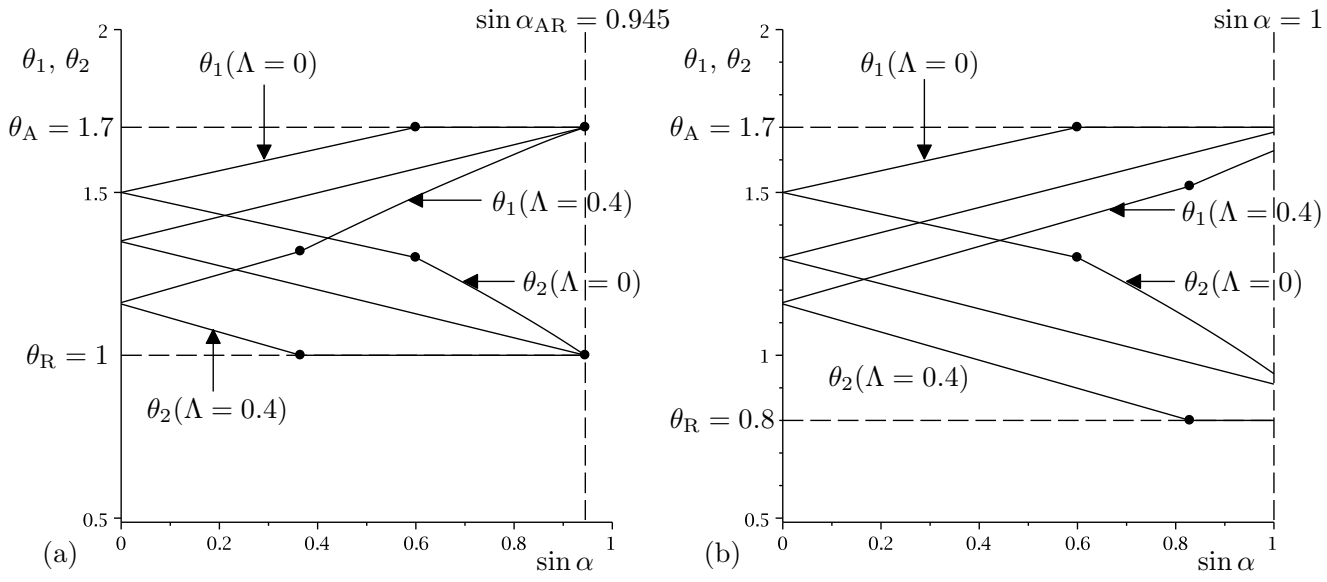

FIG. 17: Plots of the contact angles θ_1 and θ_2 as functions of $\sin\alpha$ for a small ridge for (a) $\Lambda = 0$, $\Lambda_{\rm AR} \simeq 0.19$, 0.4 when $L = 2$, $\theta_{\rm A} = 1.7$ and $\theta_{\rm R} = 1$ (for which $\sin\alpha_{\rm AR} = (\theta_{\rm A}^2 - \theta_{\rm R}^2)/(2V) = 0.945 < 1$), and for (b) $\Lambda = 0$, 0.2, 0.4 when $L = 2$, $\theta_{\rm A} = 1.7$ and $\theta_{\rm R} = 0.8$ (for which $(\theta_{\rm A}^2 - \theta_{\rm R}^2)/(2V) = 1.125 > 1$). In both (a) and (b) the leftmost dot on each curve indicates the point at which the first contact line (which can be either the upslope or the downslope contact line) de-pins, and in (b) the rightmost dot indicates the point $\sin\alpha = \sin\alpha_{\rm AR} = 0.945$ at which the second contact line de-pins.

and

$$h_{11} = \frac{Lx(L-2x)(L-x)}{48} - \frac{x^2(L-x)^2}{24}\log x + \frac{x^2(L-x)^2}{24}\log(L-x), \qquad (50)$$

respectively. The behaviours of H_0 and H_1 are qualitatively similar to those in the case of large ridge shown in Figure 2, except that when $72V/L^4 > 1$ $H_0'(L)$ is strictly positive (rather than simply non-negative) and $H_1'(0)$ is strictly negative (rather than simply non-positive).

In general, the behaviour of a small ridge can be similar to that of a large ridge described in Secs III–VI, with, as we have already seen, the important qualitative difference that, whereas for a large ridge the value of $\hat{\alpha}$ is unbounded, for a small ridge the value of $\sin\alpha$ cannot exceed unity, and hence, unlike in the case of a large ridge, for a small ridge even in the general case in which $\theta_{\rm A}$ is finite and $\theta_{\rm R}$ is non-zero one or both of the contact lines may never de-pin. For example, for a small ridge the transverse force balance (45) shows that if

the second contact line de-pins then it does so when $\sin\alpha = \sin\alpha_{\rm AR}$, where

$$\sin\alpha_{\rm AR} = \frac{\theta_{\rm A}^2 - \theta_{\rm R}^2}{2V}, \tag{51}$$

and that if there exists a critical value of Λ for which the two contact lines de-pin simultaneously, denoted again by $\Lambda_{\rm AR}$, then the value of Λ relative to $\Lambda_{\rm AR}$ determines which of the two contact lines de-pins first for increasing $\sin\alpha$. When $\sin\alpha_{\rm AR} = (\theta_{\rm A}^2 - \theta_{\rm R}^2)/(2V) \leq 1$ this behaviour is qualitatively the same as in the case of a large ridge discussed in Sec. V B; however, when $(\theta_{\rm A}^2 - \theta_{\rm R}^2)/(2V) > 1$ the second contact line never de-pins. This behaviour is illustrated in Figure 17 which shows how the contact angles θ_1 and θ_2 vary with $\sin\alpha$ for a range of values of Λ. Specifically, Figure 17(a) shows the behaviour in the case $L = 2$, $\theta_{\rm A} = 1.7$ and $\theta_{\rm R} = 1$ in which $\sin\alpha_{\rm AR} = (1.7^2 - 1)/(2V) = 0.945 < 1$, $\Lambda_{\rm AR} \simeq 0.19$, and the behaviour is qualitatively the same as that in the case of a large sessile ridge shown in Figure 11, while Figure 17(b) shows the behaviour in the case $L = 2$, $\theta_{\rm A} = 1.7$ and $\theta_{\rm R} = 0.8$ in which $(1.7^2 - 0.8^2)/(2V) = 1.125 > 1$, $\Lambda_{\rm AR}$ does not exist, and the second contact line never de-pins. In particular, closer inspection of Figure 17(b) reveals that for values of Λ less than that at which $\theta_1 = \theta_{\rm A}$ at $\sin\alpha = 1$ (exemplified by the case $\Lambda = 0$) only the downslope contact line de-pins, for values of Λ greater than that at which $\theta_2 = \theta_{\rm R}$ at $\sin\alpha = 1$ (exemplified by the case $\Lambda = 0.4$) only the upslope contact line de-pins, while for intermediate values of Λ (exemplified by the case $\Lambda = 0.2$) neither contact line ever de-pins.

VIII. CONCLUSIONS

In the present work we described the behaviour of a steady thin sessile or pendent ridge of fluid on an inclined planar substrate which is strongly coupled to the external pressure gradient arising from an external airflow that flows parallel to the substrate far from the ridge. When the substrate is nearly horizontal (specifically, when $\alpha = O(\epsilon)$ for a sessile ridge or $\pi - \alpha = O(\epsilon)$ for a pendent ridge) a relatively large ridge can be supported against gravity by capillary and/or external pressure forces, whereas when the substrate is not restricted to being nearly horizontal (specifically, when $\alpha = O(1)$) only a relatively small ridge can

be supported; classical thin-aerofoil theory was adapted to obtain the governing singular integro-differential equations for the profile of the ridge in each case.

Attention focused mainly on the case of a large sessile ridge on a nearly horizontal substrate. In Sec. III we described some basic properties of the solution, while in Secs IV and V we used a combination of asymptotic and numerical techniques to analyse the effect of varying the strength of the external airflow, Λ, and the angle of inclination of the substrate, $\hat{\alpha}$, respectively.

In Sec. IV A we studied a pinned ridge for increasing Λ and showed that the effect of strengthening the airflow is to push the ridge down near to its edges but to pull it up near to its middle. In Sec. IV B we showed that at a critical value of $\Lambda = \Lambda_{\rm R}$ the upslope contact angle reaches the receding contact angle $\theta_{\rm R}$ at which the upslope contact line de-pins, and continuing to increase Λ beyond $\Lambda_{\rm R}$ results in the de-pinned ridge becoming increasingly narrow, thick and symmetric in the limit of a strong external airflow, $\Lambda \to \infty$.

In Sec. V A we studied a pinned ridge for increasing $\hat{\alpha}$ and showed that the effect of tilting the substrate is to skew the ridge downslope. In Sec. V B we showed that, depending on the values of the advancing and receding contact angles, the ridge may first de-pin at either the upslope or the downslope contact angle but, in general, eventually both contact lines de-pin at $\hat{\alpha} = \hat{\alpha}_{\rm AR} = (\theta_{\rm A}^2 - \theta_{\rm R}^2)/(2V)$. In Secs V C and V D we considered the special cases $\theta_{\rm R} = 0$ in which only the downslope contact line de-pins, and $\theta_{\rm A} = \infty$ in which only the upslope contact line de-pins, respectively.

In Sec. VI we showed that the behavour of a large pendent ridge is qualitatively similar to that of a large sessile ridge, while in Sec. VII we showed that the important qualitative difference between the behaviour of a large ridge and a small ridge is that for the latter even in the general case in which $\theta_{\rm A}$ is finite and $\theta_{\rm R}$ is non-zero one or both of the contact lines may never de-pin.

The goal of the present work was to formulate and analyse a simple model for the strongly coupled interaction between a thin ridge of fluid and an external airflow. Clearly this analysis could be extended in several directions, such as to include detachment of the external airflow

at some point on the free surface of the ridge (as discussed by, for example, Durbin [7]) and/or a non-zero shear stress at the free surface of the ridge (as discussed by, for example, King and Tuck [8] and Sullivan et al. [26]).

IX. ACKNOWLEDGEMENTS

The first author (CP) gratefully acknowledges the financial support of the University of Strathclyde via a Postgraduate Research Scholarship. This work was begun while the second author (SKW) was a Visiting Fellow in the Oxford Centre for Collaborative Applied Mathematics (OCCAM), Mathematical Institute, University of Oxford, United Kingdom, and completed while he was a Visiting Fellow at the Isaac Newton Institute for Mathematical Sciences in Cambridge, United Kingdom as part of the programme on "Mathematical Modelling and Analysis of Complex Fluids and Active Media in Evolving Domains". This publication was based on work supported in part by Award No KUK-C1-013-04, made by King Abdullah University of Science and Technology (KAUST).

---

[1] A. C. Robertson, I. J. Taylor, S. K. Wilson, B. R. Duffy, and J. M. Sullivan. Numerical simulation of rivulet evolution on a horizontal cable subject to an external aerodynamic field. *J. Fluids Struct.*, 26:50–73, 2010.

[2] C. Lemaitre, E. de Langre, and P. Hémon. Rainwater rivulets running on a stay cable subject to wind. *Euro. J. Mech. B/Fluids*, 29:251–258, 2010.

[3] H. Kim, S. Grobe, G. E. Elsinga, and J. Westerweel. Full 3D-3C velocity measurement inside a liquid immersion droplet. *Exp. Fluids*, 51:395–405, 2011.

[4] J. A. Cuminato, A. D. Fitt, M. J. S. Mphaka, and A. Nagamine. A singular integro-differential equation model for dryout in LMFBR boiler tubes. *IMA J. Appl. Math.*, 75:269–290, 2010.

[5] F.-C. Chou and P.-Y. Wu. Effect of air shear on film planarization during spin coating. *J. Electrochem. Soc.*, 147:699–705, 2000.

[6] T. G. Myers and J. P. F. Charpin. A mathematical model for atmospheric ice accretion and water flow on a cold surface. *Int. J. Heat Mass Transf.*, 47:5483–5500, 2004.

[7] P. A. Durbin. On the wind force needed to dislodge a drop adhered to a surface. *J. Fluid Mech.*, 196:205–222, 1988.

[8] A. C. King and E. O. Tuck. Thin liquid layers supported by steady air-flow surface traction. *J. Fluid Mech.*, 251:709–718, 1993.

[9] A. C. King, E. O. Tuck, and J. M. Vanden-Broeck. Air-blown waves on thin viscous sheets. *Phys. Fluids A*, 5:973–978, 1993.

[10] F. T. Smith, P. W. M. Brighton, P. S. Jackson, and J. C. R. Hunt. On boundary-layer flow past two-dimensional obstacles. *J. Fluid Mech.*, 113:123–152, 1981.

[11] J. A. Cuminato, A. D. Fitt, and S. McKee. A review of linear and nonlinear Cauchy singular integral and integro-differential equations arising in mechanics. *J. Int. Eqns Appl.*, 19:163–207, 2007.

[12] J. A. Moriarty, L. W. Schwartz, and E. O. Tuck. Unsteady spreading of thin liquid films with small surface tension. *Phys. Fluids A*, 3:733–742, 1991.

[13] X. Li and C. Pozrikidis. Shear flow over a liquid drop adhering to a solid surface. *J. Fluid Mech.*, 307:167–190, 1996.

[14] J. J. Kriegsmann, M. J. Miksis, and J.-M. Vanden-Broeck. Pressure driven disturbances on a thin viscous film. *Phys. Fluids*, 10:1249–1255, 1998.

[15] I. S. McKinley, S. K. Wilson, and B. R. Duffy. Spin coating and air-jet blowing of thin viscous drops. *Phys. Fluids*, 11:30–47, 1999.

[16] I. S. McKinley and S. K. Wilson. The linear stability of a ridge of fluid subject to a jet of air. *Phys. Fluids*, 13:872–883, 2001.

[17] I. S. McKinley and S. K. Wilson. The linear stability of a drop of fluid during spin coating or subject to a jet of air. *Phys. Fluids*, 14:133–142, 2002.

[18] S. K. Wilson and B. R. Duffy. Unidirectional flow of a thin rivulet on a vertical substrate subject to a prescribed uniform shear stress at its free surface. *Phys. Fluids.*, 17:108105, 2005.

[19] T. G. Myers, H. X. Liang, and B. Wetton. The stability and flow of a rivulet driven by interfacial shear and gravity. *Int. J. Nonlinear Mech.*, 39:1239–1249, 2004.

[20] H. H. Saber and M. S. El-Genk. On the breakup of a thin liquid film subject to interfacial shear. *J. Fluid Mech.*, 500:113–133, 2004.

[21] N. H. Shuaib, H. Power, S. Hibberd, and K. Simmons. A numerical study of wave structures developed on the free surface of a film flowing on inclined planes and subjected to surface shear. *Int. J. Numer. Meth. Engng*, 68:755–789, 2006.

[22] N. Alleborn, A. Sharma, and A. Delgado. Probing of thin slipping films by persistent external disturbances. *Can. J. Chem. Eng.*, 85:586–597, 2007.

[23] J. P. Pascal and S. J. D. D'Alessio. Instability of power-law fluid flows down an incline subjected to wind stress. *Appl. Math. Model.*, 31:1229–1248, 2007.

[24] J. M. Sullivan, S. K. Wilson, and B. R. Duffy. A thin rivulet of perfectly wetting fluid subject to a longitudinal surface shear stress. *Q. J. Mech. Appl. Math.*, 61:25–61, 2008.

[25] S. K. Wilson, J. M. Sullivan, and B. R. Duffy. The energetics of the breakup of a sheet and of a rivulet on a vertical substrate in the presence of a uniform surface shear stress. *J. Fluid Mech.*, 674:281–306, 2011.

[26] J. M. Sullivan, C. Paterson, S. K. Wilson, and B. R. Duffy. A thin rivulet or ridge subject to a uniform transverse shear stress at its free surface due to an external airflow. *Phys. Fluids*, 24:082109, 2012.

[27] M. Van Dyke. *Perturbation Methods in Fluid Mechanics*. Parabolic, 2nd edition, 1975.

[28] E. B. Dussan V. On the ability of drops to stick to surfaces of solids. Part 3. The influences of the motion of the surrounding fluid on dislodging drops. *J. Fluid Mech.*, 174:381–397, 1987.

[29] T. D. Blake and K. J. Ruschak. *Wetting: Static and dynamic contact lines, Chapter 3 in "Liquid Film Coating", Eds S. F. Kistler and P. M. Schweizer*. Chapman and Hall, 1997.

[30] L. M. Hocking and M. J. Miksis. Stability of a ridge of fluid. *J. Fluid Mech.*, 247:157–177, 1993.

[31] D. Tseluiko, M. G. Blyth, D. T. Papageorgiou, and J.-M. Vanden-Broeck. Electrified viscous thin film flow over topography. *J. Fluid Mech.*, 597:449–475, 2008.

Appendix A: Numerical Method

In this Appendix we outline the numerical method used to solve the governing linear singular integro-differential equation (10) subject to the boundary conditions (9). We first map the ridge from the interval $x \in [0, L]$ onto the interval $x \in [0, 1]$, which is then divided into n equally spaced subintervals $[x_i, x_{i+1}]$, where $x_i = i/n$, $0 \leq i \leq n-1$. We adopt a method similar to that used by Tseluiko et al. [31] and use central differences to approximate $h'''(x)$, $h'(x)$ and the derivative of the integral term; the integral itself is approximated as half the sum of the integrals in each double subinterval $[\xi_{j-1}, \xi_{j+1}]$ for $1 \leq j \leq n-1$. Hence

the term

$$\frac{\mathrm{d}}{\mathrm{d}x}\fint_0^1 \frac{h'(\xi)}{x-\xi}\,\mathrm{d}\xi \tag{A1}$$

is discretised and approximated by

$$\begin{aligned}
& n\left(\fint_0^1 \frac{h'(\xi)}{x_{i+\frac{1}{2}}-\xi}\,\mathrm{d}\xi - \fint_0^1 \frac{h'(\xi)}{x_{i-\frac{1}{2}}-\xi}\,\mathrm{d}\xi\right) \\
= \; & \frac{n^2}{4}\sum_{j=1}^{n-1}(h_{j+1}-h_{j-1})\left(\int_{\xi_{j-1}}^{\xi_{j+1}} \frac{\mathrm{d}\xi}{x_{i+\frac{1}{2}}-\xi} - \int_{\xi_{j-1}}^{\xi_{j+1}} \frac{\mathrm{d}\xi}{x_{i-\frac{1}{2}}-\xi}\right) \\
+ \; & \frac{n^2 h_1}{2}\left(\int_{\xi_0}^{\xi_1} \frac{\mathrm{d}\xi}{x_{i+\frac{1}{2}}-\xi} - \int_{\xi_0}^{\xi_1} \frac{\mathrm{d}\xi}{x_{i-\frac{1}{2}}-\xi}\right) - \frac{n^2 h_{n-1}}{2}\left(\int_{\xi_{n-1}}^{\xi_n} \frac{\mathrm{d}\xi}{x_{i+\frac{1}{2}}-\xi} - \int_{\xi_{n-1}}^{\xi_n} \frac{\mathrm{d}\xi}{x_{i-\frac{1}{2}}-\xi}\right) \\
= \; & \frac{n^2}{4}\sum_{j=1}^{n-1}(h_{j+1}-h_{j-1})\log\left|\frac{(2i-2j+3)\,(2i-2j-3)}{(2i-2j-1)\,(2i-2j+1)}\right| \\
+ \; & \frac{n^2 h_1}{2}\log\left|\frac{(2i-3)\,(2i+1)}{(2i-1)^2}\right| + \frac{n^2 h_{n-1}}{2}\log\left|\frac{(2i-2n-1)\,(2i-2n+3)}{(2i-2n+1)^2}\right|,
\end{aligned} \tag{A2}$$

where

$$\delta x = x_{i+1}-x_i, \quad n=\frac{1}{\delta x}, \quad x_{i\pm\frac{1}{2}}=\frac{i\pm\frac{1}{2}}{n}, \quad \xi_{j\pm1}=\frac{j\pm1}{n}, \quad h_j=h(\xi_j), \tag{A3}$$

and $h_0 = h_n = 0$ from the boundary conditions. Then, rather than specifying the volume condition directly, we specify either θ_1 or θ_2 to give an expression for either h_1 or h_{n-1}, respectively. This yields a system of $(n-2)\times(n-2)$ linear equations for the ridge profile h_i at each node x_i, which is solved using the mathematical software package MAPLE. This is done iteratively; specifically, the value of the specified angle is altered until the volume condition (9) is satisfied to within a prescribed tolerance (typically 10^{-6}). The numerical results show good agreement when checked against the transverse force balance (16) and the asymptotic results derived in the present work.